



## Historical changes in $^{239}\text{Pu}$ and $^{240}\text{Pu}$ sources in sedimentary records in the East China Sea: Implications for provenance and transportation

Wang, Jinlong; Baskaran, Mark; Hou, Xiaolin; Du, Jinzhou; Zhang, Jing

*Published in:*  
Earth and Planetary Science Letters

*Link to article, DOI:*  
[10.1016/j.epsl.2017.03.005](https://doi.org/10.1016/j.epsl.2017.03.005)

*Publication date:*  
2017

*Document Version*  
Peer reviewed version

[Link back to DTU Orbit](#)

### *Citation (APA):*

Wang, J., Baskaran, M., Hou, X., Du, J., & Zhang, J. (2017). Historical changes in  $^{239}\text{Pu}$  and  $^{240}\text{Pu}$  sources in sedimentary records in the East China Sea: Implications for provenance and transportation. *Earth and Planetary Science Letters*, 466, 32-42. DOI: 10.1016/j.epsl.2017.03.005

---

### General rights

Copyright and moral rights for the publications made accessible in the public portal are retained by the authors and/or other copyright owners and it is a condition of accessing publications that users recognise and abide by the legal requirements associated with these rights.

- Users may download and print one copy of any publication from the public portal for the purpose of private study or research.
- You may not further distribute the material or use it for any profit-making activity or commercial gain
- You may freely distribute the URL identifying the publication in the public portal

If you believe that this document breaches copyright please contact us providing details, and we will remove access to the work immediately and investigate your claim.

---

1           **Historical Changes in  $^{239}\text{Pu}$  and  $^{240}\text{Pu}$  Sources in**  
2           **Sedimentary Records in the East China Sea:**  
3           **Implications for provenance and transportation**

4  
5           Jinlong Wang<sup>1</sup>, Mark Baskaran<sup>2</sup>, Xiaolin Hou<sup>3,4</sup>, Jinzhou Du<sup>1,\*</sup>, and Jing Zhang<sup>1</sup>

6  
7           <sup>1</sup>State Key Laboratory of Estuarine and Coastal Research, East China Normal  
8           University, Shanghai 200062, P. R. China

9           <sup>2</sup>Department of Geology, Wayne State University, Detroit, Michigan, 48202-3622,  
10          USA

11          <sup>3</sup>Center for Nuclear Technologies, Technical University of Denmark, Risø Campus,  
12          Roskilde 4000, Denmark

13          <sup>4</sup>Xi'an AMS Center, SKLLQG, Institute of Earth Environment, CAS, 710061, Xi'an, P.  
14          R. China

15  
16  
17  
18          (\*Corresponding author. Tel.: +86-21-62232761; Fax: +86-21-62546441. E-mail  
19          address: [jzdu@sklec.ecnu.edu.cn](mailto:jzdu@sklec.ecnu.edu.cn))

20  
21  
22  
23          **Highlights:**

- 24          ● The Yangtze River Pu input is the dominant source of Pu near the Yangtze Estuary  
25          ● The PPG input dominated the Pu mass balance in the East China Sea  
26          ● Pu is a better chronology time marker compared to  $^{137}\text{Cs}$  in the marine environment  
27          and  $^{137}\text{Cs}$  cannot be used as a reliable chronometer in marine environment.

28  
29

30  
31  
32  
33  
34  
35  
36  
37  
38  
39  
40  
41  
42  
43  
44  
45  
46  
47  
48  
49  
50  
51  
52  
53  
54  
55  
56  
57  
58  
59  
60  
61  
62  
63  
64

---

**Abstract:**

Concentrations and isotopic composition of plutonium (Pu) are widely used for its source identification and to determine transport processes of Pu-associated particulate matter and water. We investigated the concentrations of  $^{239}\text{Pu}$  and  $^{240}\text{Pu}$  and their ratios in a number of sediment samples from the East China Sea (ECS) collected in summer (August 6-28) in 2013. The  $^{239+240}\text{Pu}$  activity concentrations in surface sediment samples were found to range between 0.048 and 0.492 Bq kg<sup>-1</sup> and the  $^{240}\text{Pu}/^{239}\text{Pu}$  atom ratios showed a similar trend as that of the  $^{239, 240}\text{Pu}$  activities; the Pu atom ratios ranged from 0.158 to 0.297, and were mostly higher than the mean global fallout value of 0.18. The  $^{239, 240}\text{Pu}$  inventories in the ECS varied widely, from 2 to 807 Bq m<sup>-2</sup>, and highest values commonly found in the coastal areas. In the Yangtze Estuary, the mean  $^{239+240}\text{Pu}$  activity concentration is close to the estimated erosional input value of 0.18 Bq kg<sup>-1</sup>, and the  $^{240}\text{Pu}/^{239}\text{Pu}$  atom ratio was found to be ~0.18, which indicates that the riverine input is the dominant source of Pu for this area. However, the total annual Yangtze River input of  $^{239+240}\text{Pu}$  was estimated to be 2.4 ×10<sup>10</sup> Bq, which is small compared to the total amount of buried  $^{239+240}\text{Pu}$ , 3.1×10<sup>13</sup> Bq in the whole ECS. The Pacific Proving Ground input appears to be the dominant source of Pu to the ECS, accounting for 45%-52% of the total inventory. The fractional amount of Pu scavenged by the Kuroshio Current (KC) and Taiwan Warm Current (TWC) into ECS sediments is estimated to be ~10%. A small fraction of Pu in the ECS could have originated from the Yellow Sea, transported by coastal currents.  $^{240}\text{Pu}/^{239}\text{Pu}$  atom ratio is useful not only to obtain a better insight of the biogeochemistry influenced by the KC, but also to trace the long-range transport of other particle-reactive radionuclides. Besides, the sedimentation rates obtained based on excess  $^{210}\text{Pb}$  and the penetration depths of  $^{239+240}\text{Pu}$  agreed quite well. Compared to  $^{137}\text{Cs}$ , the  $^{239+240}\text{Pu}$  can be used as a better chronostratigraphic time marker in marine environment.

**Key words:** East China Sea; plutonium; isotopic ratio; sediment; transportation; mass balance;

---

65 **1. Introduction**

66  $^{239}\text{Pu}$  (half-life of  $2.41 \times 10^4$  yr) and  $^{240}\text{Pu}$  (half-life of  $6.56 \times 10^3$  yr) in the  
67 environment are derived from thermonuclear bomb testing (e.g., MIKE in 1952 and  
68 BRAVO in 1954), which resulted in a large amount of global fallout (e.g. Donaldson  
69 et al., 1997), nuclear accidents (e.g., Chernobyl and Fukushima) (Clark and Smith,  
70 1988; Zheng et al., 2012) and nuclear reprocessing facilities and nuclear power plants  
71 (Peirson et al., 1982). Among the transuranic elements, concentrations of plutonium  
72 isotopes ( $^{239}\text{Pu}$ ,  $^{240}\text{Pu}$ ) and their ratios have been most widely used tracers and  
73 chronometers in aqueous and terrestrial environments. Vertical profiles of Pu isotopes  
74 in coastal and lacustrine sediments provide chronology for the past 60-65 years which  
75 is useful for the reconstruction of the temporal nutrient supply variations, organic and  
76 inorganic pollution history and biological productivity (Santschi et al., 1980;  
77 Ravichandran et al., 1995; Baskaran et al., 1996). Pu, with higher particle reactivity,  
78 could also be used to validate excess  $^{210}\text{Pb}$ -based chronology in coastal areas. A  
79 comparison of the direct atmospheric fallout record of Pu (as determined from the  
80 atmospheric fallout record of  $^{90}\text{Sr}$ ) with that preserved in sediment cores is useful to  
81 infer the effects of sediment resuspension and/or mixing due to physical and/or  
82 biological processes. Moreover, the vertical distribution of Pu in sediment cores in  
83 conjunction with excess  $^{210}\text{Pb}$  is used to delineate sediment mixing rate from sediment  
84 accumulation rates (e.g., Buffoni et al., 1992; Ravichandran et al., 1995; Su and Huh,  
85 2002).

86 The  $^{240}\text{Pu}/^{239}\text{Pu}$  ratios in the marginal seas of the Pacific Ocean vary depending on  
87 the sources of plutonium; an average  $^{240}\text{Pu}/^{239}\text{Pu}$  atom ratio of global fallout is  $0.176$   
88  $\pm 0.014$  (Krey, 1976; Kelley et al., 1999), which is distinctly different from ratios of  
89  $0.33 - 0.36$  in the Pacific Proving Grounds (PPG) in the Marshall Islands (mainly  
90 Bikini and Enewetak Atolls) (Buesseler, 1997). In the North Pacific Ocean, the  
91 principal source of Pu is close-in (tropospheric) fallout from nuclear weapons testing  
92 at the PPG and global (stratospheric) fallout, and the local regional fallout of  $^{239}\text{Pu}$   
93 and  $^{240}\text{Pu}$  was estimated to be  $2.4 \text{ PBq}$  and  $2.7 \text{ PBq}$  (Hamilton, 2004), respectively. Pu  
94 from the Marshall Islands have been reported to have spread widely into the North  
95 Pacific Ocean, especially the Northwest Pacific, due to the westward flowing North  
96 Equatorial Current (NEC) (Povinec et al., 2003). The velocity of surface  
97 water-associated radionuclides transported by the NEC is approximately  $13\text{-}18 \text{ km}$   
98  $\text{day}^{-1}$  (Donaldson et al., 1997). Therefore, Pu from the PPG can be transported to long  
99 distances into the adjacent marginal seas of the western Pacific Ocean in less than one

---

100 year and can subsequently reach the East China Sea (ECS) via the Kuroshio Current  
101 (Wang and Yamada, 2005; Liu et al., 2011). Thus the characteristic  $^{240}\text{Pu}/^{239}\text{Pu}$  atom  
102 ratio makes it an important tool to track the sources of Pu in the East China Sea.

103 ECS is one of the world's typical river-dominated ocean margin systems with a  
104 large river input and complex current system. The Yangtze River is the largest river on  
105 the Eurasian continent, discharging a large amount of water and sediment into ECS,  
106 although sediment discharge has been reduced by 75% since 2000, due to the  
107 construction of impoundments (Dai et al., 2013; 2014). 40-50% of the river-derived  
108 sedimentary particles deposited near the estuary a fraction of which is subsequently  
109 transported offshore, mostly southward along the coasts of Zhejiang and Fujian  
110 Provinces (McKee, et al., 1983). The large riverine sediment discharge and complex  
111 current system result in ECS having high concentration of suspended particles, which  
112 makes East China Sea potentially act as one of most important "sinks" for Pu  
113 originated in the PPG, compared to other adjacent marginal seas of the western Pacific  
114 Ocean. On a broader context, this is relevant to other long-range transport of other  
115 particle-reactive radionuclides such as  $^{210}\text{Pb}$ ,  $^{230}\text{Th}$ ,  $^{231}\text{Pa}$ , etc. Moreover, there are  
116 limited studies on the use of Pu as a chronological tool in the ECS (Huh and Su,  
117 1999).

118 In recent years, several investigations have been carried out to determine  $^{239+240}\text{Pu}$   
119 in the ECS (Nagaya and Nakamura, 1992; Su and Huh, 1999; 2002; Wang and  
120 Yamada, 2005; Liu et al., 2011). However,  $^{239}\text{Pu}$  and  $^{240}\text{Pu}$  data in the Yangtze River  
121 catchment are very limited, which limits an accurate estimation of the contribution  
122 from the Yangtze River input, and determination of a reliable Pu mass balance for the  
123 ECS. The objective of this work is to determine the concentrations and isotopic ratios  
124 of  $^{239}\text{Pu}$  and  $^{240}\text{Pu}$  in surface sediments and sediment cores in the ECS and to  
125 investigate the sources and mass balance of Pu evaluated from the inventories of  $^{239}\text{Pu}$   
126 and  $^{240}\text{Pu}$  and their atomic ratios. Besides, the sedimentation rate estimation is  
127 conducted to compare the Pu,  $^{137}\text{Cs}$  and  $^{210}\text{Pb}_{\text{ex}}$  based chronology methods in marine  
128 environment. It is expected that this study will provide insights on the processes and  
129 mechanisms that control the transport and fate of Pu and other species that behave  
130 similar to Pu, using a simple mass balance of Pu for the ECS.

## 131 **2. Materials and Methods:**

### 132 **2.1 Study area**

133 The ECS is a marginal sea and has a very wide and flat continental shelf, with a  
134 total area of  $7.7 \times 10^5 \text{ km}^2$ , a maximum width of 640 km, and a mean water depth of

---

135 72 m. The major current system in the ECS is very complicated, as was described in  
136 Su (2001) (Fig. 1). The freshwater from the Yangtze River flows into the estuary and  
137 subsequently flows towards the south in winter and turns to the northeast in summer.  
138 In the southern part, there are two northward currents of which one is the warm and  
139 salty Kuroshio Current (KC) along the continental shelf break of the ECS, with a  
140 branch turning into the Yellow Sea known as the Yellow Sea Warm Current (YSWC),  
141 and the other is the Taiwan Warm Current (TWC) moving northward from the  
142 Taiwan strait. Along the coast, the southeastern North Jiangsu Coastal Current  
143 (NJCC) flows to the north of the Yangtze River mouth and the southwestern  
144 Zhejiang-Fujian Coastal Current (ZFCC) flows to the south of the Yangtze River  
145 mouth. In summer, the northward TWC intensifies and the southward ZFCC weakens  
146 under the prevailing southeast monsoon. The Yellow Sea Coastal Current (YSCC) is  
147 parallel to the NJCC in the middle of the Yellow Sea and intersects with the YSWC  
148 and the TWC to form a counterclockwise circulation.

## 149 **2.2. Sampling and analysis**

150 Sediment samples, including 23 surface sediments (0-2 cm) and 6 sediment cores  
151 (Fig. 1b), were collected during the R/V “Dongfanghong 2” Cruise in August of 2013  
152 using a box corer. The sediment cores were collected with 10-cm diameter Plexiglas  
153 core tubes and were sliced in 1-cm interval using a stainless steel knife and were  
154 stored in resealable plastic bags at 4 °C until laboratory analysis. Visual observations  
155 of the cores were also recorded.

156 An aliquot of 2 g of dry sediment equivalent was used for the measurement of  
157 grain size using a laser particle analyzer (LS100Q, Beckman, USA). 60-120 g dried  
158 sample was homogeneously pulverized and sealed in a plastic container (70 mm  
159 diameter × 70 mm height) for at least three weeks to establish a secular equilibrium  
160 between  $^{226}\text{Ra}$  and daughter products of  $^{222}\text{Rn}$  before measurement. The activity  
161 concentrations of  $^{210}\text{Pb}_{\text{ex}}$  in sediment samples were measured following the method  
162 described by Du et al. (2010). The activities of  $^{137}\text{Cs}$ ,  $^{226}\text{Ra}$  and  $^{210}\text{Pb}$  were measured  
163 using HPGe  $\gamma$ -ray spectrometry (Canberra Be3830) with 35% relative counting  
164 efficiency and had an energy resolution of 1.8 keV (at 1332 keV) (Du et al., 2010).  
165 The activity of  $^{210}\text{Pb}_{\text{ex}}$  was calculated from the measured total  $^{210}\text{Pb}$  (46.5 keV,  
166 branching ratio: 4.25%) minus the parent-supported  $^{210}\text{Pb}$  activity which is assumed to  
167 be the same as the  $^{226}\text{Ra}$  activity.  $^{226}\text{Ra}$  was determined using the gamma line at 351.9  
168 keV (37.6%) for  $^{214}\text{Pb}$  and 609.3 keV (46.1%) for  $^{214}\text{Bi}$ . The activity of  $^{137}\text{Cs}$  was  
169 determined from the gamma ray peak at 661.6 keV (85%). The efficiency calibration

---

170 of the detector system was conducted using both the Laboratory Sourceless  
171 Calibration Software (LabSOCS) and sediment standard (GBW04127= was diluted by  
172 homogeneously mixed with natural marine sediment ( $< 63 \mu\text{m}$ ); the activities of the  
173 radionuclides were certified by producer (e.g., Dai et al., 2011; Wang et al., 2016a).

174 The separation method of Pu was modified from Xu et al. (2014). Briefly, 5-20 g  
175 dried sediment samples were first ashed at  $550 \text{ }^\circ\text{C}$  overnight. After spiking with 6-10  
176 mBq  $^{242}\text{Pu}$  (NIST-SRM-4334G), the residue was leached with 50-200 mL aqua regia  
177 at  $200 \text{ }^\circ\text{C}$  for 2 h. After filtration through a GF/A filter, plutonium in the leachate was  
178 coprecipitated with iron hydroxides by adding  $\text{NH}_3\text{OH}$ . The precipitate was separated  
179 by centrifugation. The precipitate was washed with  $2 \text{ mol L}^{-1}$  NaOH and then was  
180 dissolved with  $\sim 3 \text{ mL}$  of concentrated HCl. To this solution,  $\sim 650 \text{ mg}$  of  $\text{K}_2\text{S}_2\text{O}_5$  was  
181 added to reduce the overall Pu to Pu(III). The pH of the solution was adjusted to  
182  $\sim 9$ -10 by adding ammonium. The precipitate was separated by centrifugation and then  
183 dissolved with  $\sim 4 \text{ mL}$  of concentrated HCl and  $3 \text{ mL}$  of concentrated  $\text{HNO}_3$  for the  
184 oxidation of Pu(III)–Pu(IV) by  $\text{NO}_2^-$  in the  $\text{HNO}_3$  solution. The solution was gently  
185 evaporated to near dryness and  $5 \text{ mL}$  of  $8 \text{ mol L}^{-1}$   $\text{HNO}_3$  was added to dissolve the  
186 residue. The solution was loaded on to a preconditioned AG 1- $\times$ 4 anion-exchange  
187 column ( $1.0 \text{ cm}$  in diameter and  $20\text{-cm}$  height,  $50$ - $100$  mesh,  $\text{Cl}^-$  form). After rinsing  
188 the column with  $8 \text{ mol L}^{-1}$   $\text{HNO}_3$  and  $9 \text{ mol L}^{-1}$  HCl to remove most uranium, thorium  
189 and other matrix elements, Pu was eluted with  $70 \text{ mL}$  of  $0.5 \text{ mol L}^{-1}$  HCl. Pu in the  
190 eluate was co-precipitated with  $\text{Fe}(\text{OH})_3$  after adding  $100 \text{ mg}$  of  $\text{Fe}^{3+}$  ( $\text{FeCl}_3$ ), then the  
191 redox pair of  $\text{K}_2\text{S}_2\text{O}_5$ -conc.  $\text{HNO}_3$  was used to adjust overall Pu to Pu(IV). The final  
192 sample solution prepared in  $1 \text{ mol L}^{-1}$   $\text{HNO}_3$  was loaded to a TEVA column ( $2 \text{ mL}$ ,  
193  $200$  mesh). After rinsing with  $60 \text{ mL}$  of  $1 \text{ mol L}^{-1}$   $\text{HNO}_3$  and  $60 \text{ mL}$  of  $6 \text{ mol L}^{-1}$  HCl,  
194 Pu was finally eluted with  $40 \text{ mL}$  of  $0.1 \text{ mol L}^{-1}$   $\text{NH}_2\text{OH}\cdot\text{HCl}$  in  $2 \text{ mol L}^{-1}$  HCl. The  
195 elute was evaporated to dryness on a hot-plate followed by adding  $7$ - $10 \text{ mL}$  of  
196 concentrated nitric acid and heating at  $200 \text{ }^\circ\text{C}$  to decompose the hydroxylamine  
197 hydrochloride. The residue was finally dissolved in  $0.5 \text{ mol L}^{-1}$   $\text{HNO}_3$  and In (III) (as  
198  $\text{InCl}_3$ ) was added as an internal standard for measurement of  $^{239}\text{Pu}$  and  $^{240}\text{Pu}$  by the  
199 ICP-MS (X Series II, Thermo Fisher Scientific, Waltham, MA) equipped with an  
200 Xs-skimmer cone and an ultrasonic nebulizer (U5000AT+, CETAC, USA) under hot  
201 plasma conditions. The chemical yield was found to range between  $64\%$  and  $96\%$   
202 (mean:  $72\% \pm 16\%$ ). Determination of  $^{239}\text{Pu}$  and  $^{240}\text{Pu}$  in separated samples was  
203 conducted using an inductively coupled plasma mass spectrometer (ICP-MS) The  
204 separation of Pu using anion exchange chromatography followed by extraction

---

205 chromatography (TEVA column) ensures sufficient removal of uranium, which  
206 interferes the measurement of  $^{239}\text{Pu}$  by tailing and  $^1\text{H}^{238}\text{U}$  ion. Uranium remained in  
207 the separated sample was monitored by measurement of  $^{238}\text{U}$  to be less than 0.02ppb  
208 (for detailed information, Qiao et al., 2014 and Xu et al., 2014). A certified reference  
209 material (IAEA-376, marine sediment) was analyzed with the samples, and the  
210 analytical results of  $^{239}\text{Pu}$  and  $^{240}\text{Pu}$  agree well with the certified values.

### 211 3. Results and discussions

#### 212 3.1. The spatial distribution of Pu isotopes in surface sediments of the ECS

213 The activity concentrations of Pu isotopes and  $^{210}\text{Pb}_{\text{ex}}$  along with grain size are  
214 given in the supplementary material. The  $^{239+240}\text{Pu}$  activity concentrations in surficial  
215 sediments (Fig. 2c) ranged between  $0.048\pm 0.004$  and  $0.492\pm 0.035$  Bq  $\text{kg}^{-1}$  (mean:  
216  $0.188\pm 0.119$  Bq  $\text{kg}^{-1}$ ). The activity concentration of  $^{239}\text{Pu}$  and  $^{240}\text{Pu}$  varied between  
217  $0.026\pm 0.003$  and  $0.246\pm 0.025$  Bq  $\text{kg}^{-1}$  (mean:  $0.099 \pm 0.057$ ) and  $0.022\pm 0.002$  and  
218  $0.247\pm 0.025$  Bq  $\text{kg}^{-1}$  (mean:  $0.088 \pm 0.061$  Bq  $\text{kg}^{-1}$ ), respectively (Fig. 2a, b). The  
219 spatial distribution of radionuclides activities (Fig. 2) were produced by the Surfer  
220 mapping software package using Kriging interpolation based on a digital elevation  
221 model (DEM) with  $6 \times 6$  km grid resolution. The lowest Pu concentrations were  
222 observed near the Yangtze Estuary and Hangzhou Bay, with a range of  $0.048\pm 0.004$   
223 to  $0.186\pm 0.014$  Bq  $\text{kg}^{-1}$ . The sedimentation rate in these regions showed higher values  
224 of  $> 2$  cm  $\text{y}^{-1}$  (Huh and Su, 1999), so the low  $^{239+240}\text{Pu}$  activity is likely related to  
225 dilution of massive influx of river-borne sediments. The Pu concentrations in  
226 sediments north of the ECS region were also low. A decreasing trend of  $^{239+240}\text{Pu}$   
227 concentrations in sediments from the offshore towards the northwest was also  
228 observed, which is similar to the direction of the YSWC. In contrast, the maximum  
229  $^{239+240}\text{Pu}$  concentration was observed on the transportation pathway of the TWC and  
230 decreased towards inshore, suggesting that the TWC likely plays an important role in  
231 the transport of Pu from the open sea. The measured  $^{239}\text{Pu}$  and  $^{240}\text{Pu}$  concentrations in  
232 surface sediment in this work are comparable to the reported values in the ECS and  
233 other marginal seas of the Pacific Ocean such as the Yellow Sea ( $0.13 - 0.35$  Bq  $\text{kg}^{-1}$ ,  
234 mean:  $0.23$  Bq  $\text{kg}^{-1}$ ) (Nagaya and Nakamura, 1992) and the South China Sea ( $0.16 -$   
235  $0.79$  Bq  $\text{kg}^{-1}$ , mean:  $0.50$  Bq  $\text{kg}^{-1}$ ) (Wu et al., 2014) but are much lower than the  
236 values observed in the Okinawa Trough ( $1.4 - 2.5$  Bq  $\text{kg}^{-1}$ , mean:  $1.8$  Bq  $\text{kg}^{-1}$ ) (Wang  
237 and Yamada, 2005) and the northwest Pacific Ocean ( $0.15 - 5.4$  Bq  $\text{kg}^{-1}$ , mean:  $2.4$  Bq  
238  $\text{kg}^{-1}$ ) (Moon et al., 2003). This variation in different areas may indicate a pathway of  
239 Pu from the PPG transported by the NEC and the KC.



---

### 240 **3.2 Distribution of $^{240}\text{Pu}/^{239}\text{Pu}$ atom ratios and sources term of Pu in the ECS**

241 The  $^{240}\text{Pu}/^{239}\text{Pu}$  atom ratios in sediment cores from the ECS (Fig. 2d) ranged  
242 from  $0.158\pm 0.022$  to  $0.297\pm 0.042$  (mean:  $0.238\pm 0.036$ ), which was between global  
243 fallout value of  $0.18 \pm 0.02$  (Krey et al., 1976) and PPG close-in fallout value of  
244  $0.33\text{-}0.36$  (Buesseler, 1997). The major inputs of Pu to this area is likely derived from:  
245 1) atmospheric fallout from weapons testing, 2) the close-in fallout (tropospheric) in  
246 PPG, 3) riverine input from the erosion and leaching of soils in the watershed of  
247 Yangtze River, 4) emission from the nuclear reprocessing plants, 5) nuclear accidents  
248 (e.g. Chernobyl and Fukushima accidents) and 6) transport of effluents from adjacent  
249 sea area (e.g., Yellow Sea).

#### 250 **3.2.1 The close-in fallout and emission from the nuclear power plants**

251 From Figure 3, the distribution of  $^{240}\text{Pu}/^{239}\text{Pu}$  atom ratios were  $\sim 0.18$  in Chinese  
252 (Zheng et al., 2009; Dong et al., 2010; Liu et al., 2013; Bu et al., 2014) and Japanese  
253 soils profiles (Muramatsu et al., 1999, 2003), which implies that the direct input from  
254 the close-in fallout from Semipalatinsk, Lop Nur nuclear tests and Chernobyl and  
255 Fukushima accidents did not give a significant contribution to the source of Pu in  
256 these areas, due to their distinctive  $^{240}\text{Pu}/^{239}\text{Pu}$  atom ratios of  $0.03\text{-}0.05$  (Beasley et al.,  
257 1998),  $< 0.1$  (Wu et al., 2010),  $0.31\text{-}0.40$  (Boulyga et al., 1997) and  $0.32\text{-}0.33$  (Zheng  
258 et al., 2012), respectively. Considering the location of the ECS is far away from the  
259 any sites of nuclear weapons testing, and the catchment of the rivers flowing into the  
260 ECS is also far from the Chinese weapons testing site, Pu contribution from the  
261 close-in fallout of the Chinese weapons testing appears to be negligible here. There  
262 were 14 nuclear power reactors (as of August 2013) operating along the Chinese coast  
263 in the ECS. However, all Pu was produced and confined in the fuel elements, and  
264 there is no report on the leakage of nuclear fuel from any of these NPPs, the  
265 contribution from the Chinese NPPs would be negligible.

#### 266 **3.2.2 Riverine input from the erosion and leaching of soils**

267 The Yangtze River and the Yellow River load huge amounts of sediments to  
268 China's marginal seas and are the potential riverine source of  $^{239,240}\text{Pu}$  to the ECS. It  
269 has been reported that the  $^{240}\text{Pu}/^{239}\text{Pu}$  atom ratios in both of these river catchments  
270 are  $0.18$  (Zheng et al., 2009; Dong et al., 2010; Bu et al., 2014) and that the riverine  
271 Pu eventually originates from the global atmospheric fallout. Moreover, there are  
272 several small rivers that flow into the ECS from the Zhe-Min coast but the  
273 contributions from these rivers are likely negligible considering the relatively small  
274 amount of water and sediment discharge (e.g., the largest catchment of all smaller

---

275 rivers, streams and tributaries is Min River catchment with an area of 61,000 km<sup>2</sup>,  
276 CWRC, 2013). Because of very limited published Pu data in the Yangtze watershed,  
277 the reported river-borne input of <sup>239+240</sup>Pu has high uncertainty. Recently, some  
278 investigations of Pu isotopes in soils and sediments of the Yangtze river catchment  
279 (Liao et al, Dong et al., 2010; Bu et al., 2014) have been conducted, which enables us  
280 to obtain a better estimation of the river input of Pu. Smith et al. (1987) and Dominik  
281 et al. (1987) investigated several catchments and estimated the residence time of Pu  
282 from soil to be 800-3,000 yr. The Yangtze catchment is one of the largest river  
283 catchments in the world and contains many dams (e.g., The Three Gorges Dam);  
284 therefore, we used the largest value of the range (3,000 yr) as the watershed residence  
285 time of Pu. It can be calculated that 0.023% of the Pu in the drainage catchment is  
286 eroded each year. The Yangtze River input of <sup>239+240</sup>Pu was calculated following the  
287 equation (modified from previous studies: Ravichandran et al., 1995; Baskaran et al.,  
288 1997):

$$289 \quad I_{Pu} = A_d * I_f * f_e \quad (1)$$

290 where  $A_d$  is the area of the catchment ( $1.8 \times 10^{12} \text{ m}^2$ ),  $I_f$  is the inventory of <sup>239+240</sup>Pu  
291 ( $\text{Bq m}^{-2}$ ) and  $f_e$  is the fraction of the inventory of <sup>239+240</sup>Pu eroded each year (0.023%).  
292 The inventories of <sup>239+240</sup>Pu in soils of the Yangtze catchment listed in Table 2 range  
293 from  $19.0 \pm 1.6$  to  $114 \pm 5.9 \text{ Bq m}^{-2}$  (arithmetic mean:  $59 \pm 35 \text{ Bq m}^{-2}$ ). The mean Pu  
294 input derived from the Yangtze River was calculated to be  
295  $(0.79 \pm 0.07) \times 10^{10}$ - $(4.7 \pm 0.2) \times 10^{10} \text{ Bq y}^{-1}$  (arithmetic mean:  $(2.4 \pm 1.4) \times 10^{10} \text{ Bq y}^{-1}$ ).  
296 The Yangtze River delivers approximately  $1.3 \times 10^8 \text{ tons yr}^{-1}$  of terrestrial sediment to  
297 the ECS (CWRC, 2013). Therefore, the mean <sup>239+240</sup>Pu activity concentration in the  
298 suspended materials eroded from the drainage area was calculated to be  $0.06 \pm 0.01$  -  
299  $0.36 \pm 0.02 \text{ Bq kg}^{-1}$  (mean:  $0.18 \pm 0.10 \text{ Bq kg}^{-1}$ ), which was close to the values of  
300 surface sediments near the Yangtze Estuary and Hangzhou Bay (Fig. 3). Considering  
301 the <sup>240</sup>Pu/<sup>239</sup>Pu atom ratios are  $\sim 0.18$  in this area, we suggest that the Yangtze River  
302 input is the main source of Pu isotopes for the estuarine area in the ECS. Liu et al.  
303 (2011) also suggested that the dilution of riverine input played an important role in the  
304 distribution of Pu isotopes near the Yangtze Estuary (Liu et al., 2011). The magnetic  
305 minerals and particulate heavy metals in this area have also been reported to be from  
306 the Yangtze River input (Che et al., 2003; Liu et al., 2010). This is because  $\sim 50\%$  of  
307 the Yangtze River-derived fine sediments were deposited near the Yangtze Estuary  
308 and Hangzhou Bay under the cumulative action of delivery by the CDW and the  
309 barrier effect from the northward flowing TWC (Che et al., 2003; Liu et al., 2006).

310 All these observations support that soil erosion in the Yangtze River catchment  
311 contributes the major fraction of Pu to the estuarine sediment.

### 312 **3.2.3 Long-range transport from the PPG**

313 Fukushima accident has been reported to release a very small amount of Pu to  
314 marine environment (Zheng et al., 2012), thus the long distance transport from  
315 Fukushima coastal waters to the ECS is negligible. However, the Pu derived from the  
316 PPG transport has been suggested to be an important source of  $^{239+240}\text{Pu}$  (Lee et al.,  
317 2004; Zheng and Yamada, 2004; Wang and Yamada, 2005; Liu et al., 2011). The  
318 distribution of  $^{240}\text{Pu}/^{239}\text{Pu}$  atom ratios in surficial sediments (including sediment  
319 cores) and seawater (Fig. 3) around the NEC and KC pathway showed a similar  
320 variation pattern with a mean atom ratio of  $\sim 0.24$  (e.g., Kim et al., 2004; Zheng and  
321 Yamada, 2004; Yamada et al., 2006). A strong signature of the PPG Pu was recorded  
322 in a natural coral of Guam site with a mean atom ratio of 0.31 (Lindahl et al., 2011).  
323 The spatial distribution of the  $^{240}\text{Pu}/^{239}\text{Pu}$  atom ratio coincided with the water mass  
324 distribution in the ECS, which apparently shows the influence of transport of Pu from  
325 PPG inputs by the Kuroshio Current and the TWC. These observations further support  
326 that Pu could transport from the PPG into the ECS. As a particle-reactive nuclide in  
327 marine environment, the dissolved Pu in ECS can be removed from the water column  
328 into sediments by particle scavenging, after the advective lateral transport from the  
329 open ocean to the ocean margin (Zheng and Yamada, 2006).

330 The riverine input and global fallout  $^{239+240}\text{Pu}$  can be regarded as one  
331 end-member considering their same  $^{240}\text{Pu}/^{239}\text{Pu}$  atomic ratios. A simple two  
332 end-member mixing model described by Krey et al. (1976) was used to estimate the  
333 relative contribution of plutonium isotopes from global fallout and PPG in the ECS:

$$334 \frac{(Pu)_P}{(Pu)_G} = \frac{(R_G - R_E)(1 + 3.68R_P)}{(R_E - R_P)(1 + 3.68R_G)} \quad (2)$$

335 where (Pu) and R represent the  $^{239+240}\text{Pu}$  activity concentration and the  $^{240}\text{Pu}/^{239}\text{Pu}$   
336 atom ratio, respectively. The subscripts P, G and E refer to the PPG, global fallout,  
337 and the ECS, respectively. The constant 3.68 is the ratio of the decay constant of  
338  $^{240}\text{Pu}/^{239}\text{Pu}$  which is used to convert the activity ratio to the atomic ratio. The  $R_G$  and  
339  $R_P$  are 0.18 and 0.33-0.36, respectively (Krey et al. 1976; Buesseler, 1997). The  
340 calculated results showed that the contributions of Pu from the PPG to surface  
341 sediment of the ECS ranged from  $< 1\%$  to  $72\% \pm 7\%$ , with mean value of  $41\% \pm 6\%$   
342 ( $R_P = 0.36$ ), and from  $< 1\%$  to  $82\% \pm 8\%$ , with mean value of  $47\% \pm 7\%$  ( $R_P = 0.33$ ).  
343 Apparently, the PPG input had a great influence on the sedimentary Pu in the ECS

---

344 and is found to be the main source of Pu to the ECS.

### 345 **3.3. Temporal Variations of Pu in the sediment cores in the ECS**

#### 346 **3.3.1 Sedimentation rates**

347 The detailed information of vertical profiles of Pu isotopes are listed in  
348 supplemental file (Table A. 2). Assuming that the sedimentation rates did not change  
349 drastically over the past 61 years, the linear sedimentation rates obtained from the  
350 vertical profiles of  $^{210}\text{Pb}_{\text{ex}}$  in the ECS were:  $0.83\pm 0.48$ ,  $0.77\pm 0.10$ ,  $0.32\pm 0.03$ ,  
351  $0.38\pm 0.07$ ,  $0.13\pm 0.01$  and  $0.13\pm 0.02$   $\text{cm y}^{-1}$  at C1, E1, M7, B6, C12 and F8 sites,  
352 respectively (Fig. 4). The depth corresponding to maximum  $^{239+240}\text{Pu}$  activity  
353 concentration varied in these cores due to variable sedimentation rates. The relatively  
354 low resolution of Pu in sediment cores prevented us from identifying the exact depth  
355 layer where the  $^{239+240}\text{Pu}$  concentration peak corresponding to 1963 which would have  
356 resulted in getting better mean sedimentation rate. The penetration depths of Pu  
357 corresponding to 1952, when many high yield nuclear weapons tests were started (i.e.  
358 PPG), can be used as a chronological marker to determine independent sedimentation  
359 rate. The lowest  $^{239+240}\text{Pu}$  concentrations measured in the bottom layers of cores E1,  
360 M7, B7, C12 and F8 (Fig. 5) are near the detection limits of  $^{239+240}\text{Pu}$  ( $0.01$   $\text{Bq kg}^{-1}$ ).  
361 These bottom layers could be seen as the penetration depths of Pu corresponding to  
362 1952. Considering the uncertainty (1.5 cm) from sedimentary particle compaction  
363 during sub-sectioning, the estimated mean sedimentation rates were estimated to be  
364  $0.78\pm 0.02$ ,  $0.38\pm 0.02$ ,  $0.35\pm 0.02$ ,  $0.20\pm 0.02$  and  $0.14\pm 0.02$   $\text{cm y}^{-1}$  at E1, M7, B6, C12  
365 and F8, respectively. The discernible concentration peak for  $^{137}\text{Cs}$  corresponding to  
366 1963 was not observed in six cores (Fig. 4). This observation is due to the higher  
367 mobility of  $^{137}\text{Cs}$  due to low  $K_d$  ( $< 500$ ) in marine systems (Cochran et al., 1995;  
368 Delfanti et al., 2003; Wang et al., 2016). We attempted to use the penetration depths of  
369  $^{137}\text{Cs}$  in C12 (4.5-6.5 cm) and F8 (4.5-6.5 cm) to roughly estimate the sedimentation  
370 rates to be  $0.09\pm 0.05$   $\text{cm y}^{-1}$  at these two cores, but these rates are not reliable.

371 C1 is located near the river mouth, where there is reworked mobile mud and  
372 sediment commonly undergoes erosion (Yang et al., 2011; Wang et al., 2016). Thus,  
373 the estimated sedimentation rate of the C1 core by  $^{210}\text{Pb}_{\text{ex}}$  is less reliable and  
374 significantly lower than the reported value of  $3.0$   $\text{cm y}^{-1}$  (Su and Huh, 2002).  
375 Considering the high sedimentation rate and short length of core C1 (42 cm), it is not  
376 able to evaluate the sedimentation rate of C1 by  $^{239+240}\text{Pu}$  or  $^{137}\text{Cs}$ . The sedimentation  
377 rates estimated in this work using Pu isotopes are comparable to the data published in  
378 literature ( $0.5 - 0.8$   $\text{cm y}^{-1}$  for E1,  $0.3 - 0.5$   $\text{cm y}^{-1}$  for M7 and B6,  $0.1 - 0.2$   $\text{cm y}^{-1}$  for

379 C12 and F8, Su and Huh, 2002). The sedimentation rates estimated by  $^{137}\text{Cs}$  were  
380 much lower than those based on  $^{239+240}\text{Pu}$  and  $^{210}\text{Pb}_{\text{ex}}$  in core C12 and F8. This is  
381 likely related to the longer residence time of  $^{137}\text{Cs}$  in ocean water and  $^{137}\text{Cs}$  does not  
382 trace sedimentary particles (Lee et al., 2004). However, the sedimentation rates  
383 estimated by  $^{239+240}\text{Pu}$  agree well with those by  $^{210}\text{Pb}_{\text{ex}}$  in the other 5 cores ( $R^2=0.97$ ,  
384  $p<0.01$ ). Compared to  $^{137}\text{Cs}$ ,  $^{239+240}\text{Pu}$  is a better time marker to validate the  $^{210}\text{Pb}_{\text{ex}}$   
385 chronology in marine environment and  $^{137}\text{Cs}$  is not suitable chronometer in marine  
386 environment.

### 387 **3.3.2 The vertical variations of Pu isotope composition in the sediment cores**

388 The vertical distribution of  $^{240}\text{Pu}/^{239}\text{Pu}$  atom ratios in the sediment cores (Fig. 5  
389 and Table A. 5) shows that the Pu derived from PPG is the major source of Pu in the  
390 ECS (except C1), with a PPG contribution portion of  $> 50\%$  in most layers ( $R_p =$   
391  $0.33$ ). The atomic ratio of  $^{240}\text{Pu}/^{239}\text{Pu}$  in deep layers of cores E1, B6 and F8 varied  
392 between 0.269 and 0.314, which are close to those observed in the close-in fallout at  
393 the PPG. The trend of mean  $^{240}\text{Pu}/^{239}\text{Pu}$  atomic ratios in the sediment cores in the ECS  
394 ( $E1 > C1$ ,  $F8 > B6 > M7$ ; Table 2) are consistent with the flow direction of the TWC  
395 and the KC in the ECS. Both F8 and C12 are located in the pathway of the KC and  
396 continental shelf margin, but  $^{240}\text{Pu}/^{239}\text{Pu}$  atom ratios in C12 were relatively lower than  
397 that in F8. A previous study also reported a lower value in the upper layer of a  
398 sediment core in the same area (SST1, 0.21-0.26, Wang and Yamada, 2005), which  
399 may be attributed to other input source of Pu with lower  $^{240}\text{Pu}/^{239}\text{Pu}$  atom ratio (e.g.,  
400 terrestrial input) for C12. C12 is located in the north Okinawa Trough, which is one of  
401 important sinks of fine sedimentary particles in the ECS. Previous studies have  
402 suggested that these fine particles in the north Okinawa trough were mostly derived  
403 from terrestrial particles input, including Yangtze input and finer particles from  
404 Taiwan (e.g., Oguri et al., 2003; Dou et al., 2010; Li et al., 2015). As has been  
405 discussed above, these terrestrial particles had a lower  $^{240}\text{Pu}/^{239}\text{Pu}$  atom ratio of 0.18.  
406 Therefore, the lower  $^{240}\text{Pu}/^{239}\text{Pu}$  atom ratio was observed in the north Okinawa  
407 trough.

### 408 **3.4. Inventory of Pu in the ECS sediment cores**

409 The inventories of Pu ( $= ^{239}\text{Pu}$  inventory +  $^{240}\text{Pu}$  inventory) and  $^{210}\text{Pb}_{\text{ex}}$  were  
410 obtained from the activity in the measured layers and the interpolated activity for  
411 those layers where the radionuclides were not measured (inventory for a layer =  
412 activity in that layer (or interpolated activity for that layer)  $\times$  mass depth of that layer).  
413 The calculated inventories for total Pu and the excess  $^{210}\text{Pb}$  are:  $35.6\pm 2.5$ ,  $118\pm 5.0$ ,  
414  $65.4\pm 2.5$ ,  $58.3\pm 4.6$ ,  $33.9\pm 0.7$ ,  $1.9\pm 0.1$  Bq  $\text{m}^{-2}$  and  $12.3\pm 1.5$ ,  $14.9\pm 2.1$ ,  $6.7\pm 5.4$ ,

415 13.1±1.2, 29.2±1.6, 3.2±0.9 kBq m<sup>-2</sup> at C1, E1, M7, B6, C12 and F8, respectively.  
416 The estimated inventories of <sup>239+240</sup>Pu and mean <sup>240</sup>Pu/<sup>239</sup>Pu atom ratios in this and  
417 previous study are summarized in Table 1. Combined with the previously reported  
418 data (Table 1), the <sup>239+240</sup>Pu inventory in the ECS varied widely, from 2±0.1 to 807±7  
419 Bq m<sup>-2</sup>. Higher inventories, with two peak values in the Yangtze Estuary and the  
420 south Hangzhou Bay (Fig. 6), have been observed and are apparently higher than  
421 those expected from direct atmospheric deposition (36 - 42 Bq m<sup>-2</sup>) at 20 °N - 40 °N  
422 (Kelley et al. 1999); this is likely due to the intense scavenging of particle-reactive  
423 radionuclides resulting from higher particle fluxes in these two areas (Che et al., 2003;  
424 Huang et al., 2013). Both <sup>239+240</sup>Pu and <sup>210</sup>Pb<sub>ex</sub> inventories in core E1 were lower than  
425 the reported values in the same area prior to 1999 (Fig.1, 420 Bq m<sup>-2</sup> and 21 kBq m<sup>-2</sup>  
426 for <sup>239+240</sup>Pu and <sup>210</sup>Pb<sub>ex</sub>, respectively; Su and Huh, 1999). There is steady sediment  
427 supply to the Zhe-Min coast carried by ZFCC each year, thus, the inventory reduction  
428 in the Zhe-Min coast was not likely caused by sediment erosion; instead, the notable  
429 sediment focusing indicated by the <sup>234</sup>Th in this region may result in this reduction  
430 (Wang et al., 2016) in some areas and increased inventories in other areas, depending  
431 on the bottom water currents. However, the reduction of Yangtze sediment discharge  
432 has been suggested to lead to the erosion occurring in the Yangtze Estuary during past  
433 decade (Yang et al., 2011). In Yangtze Estuary, the erosion is likely one of the  
434 important reasons for the reduction in the sedimentary <sup>239+240</sup>Pu inventory, from 807  
435 Bq m<sup>-2</sup> obtained in 1997 (BC16, Su and Huh, 2002) to ~400 Bq m<sup>-2</sup> obtained in 2006  
436 (station 18 and SC07, Liu et al., 2011; Pan et al., 2011).

437 In order to estimate the PPG Pu contribution to sediment column of the ECS, the  
438 mean value of <sup>240</sup>Pu/<sup>239</sup>Pu atom ratios in sediment cores were calculated using the  
439 equation:

$$440 \quad R = \frac{\lambda_2 W_1}{\lambda_1 W_2} \quad (3)$$

441 where W<sub>1</sub> and W<sub>2</sub> are the inventory (Bq m<sup>-2</sup>) of <sup>240</sup>Pu and <sup>239</sup>Pu, respectively, and λ<sub>1</sub>  
442 and λ<sub>2</sub> are the decay constants of <sup>240</sup>Pu (2.89×10<sup>-7</sup> s<sup>-1</sup>) and <sup>239</sup>Pu (7.88×10<sup>-8</sup> s<sup>-1</sup>),  
443 respectively. The calculated <sup>240</sup>Pu/<sup>239</sup>Pu atom ratios are given in Table 1, together with  
444 the data from published literature. The values range from 0.223 ± 0.022 to 0.300 ±  
445 0.012 (mean: 0.247 ± 0.021). Using these values, the Pu contribution from the PPG  
446 input was estimated to be 45%±4% (R<sub>p</sub>=0.36) - 52%±4% (R<sub>p</sub>=0.33) based on the  
447 geometric mean value (0.247±0.021) of <sup>240</sup>Pu/<sup>239</sup>Pu atom ratio (Table 1).

### 448 3.5 The mass balance of Pu in the ECS sediments

---

449 The sources of Pu buried in the ECS potentially include Yangtze River input,  
450 global fallout in ECS, PPG input and the Pu derived adjoining the ECS waterbodies.  
451 A simple mass balance was used to estimate the contribution of Pu from different  
452 sources. The total surface area of ECS corresponding to the  $^{239+240}\text{Pu}$  inventories was  
453 estimated by Google Earth to be  $3.28 \times 10^{11} \text{ m}^2$ . The inventory of  $^{239+240}\text{Pu}$  from global  
454 fallout was reported to be  $36 \text{ Bq m}^{-2}$  between  $20^\circ\text{N}$  and  $30^\circ\text{N}$  and  $42 \text{ Bq m}^{-2}$  between  
455  $30^\circ\text{N}$  and  $40^\circ\text{N}$  (UNSCEAR, 2000); here we used the mean value ( $39 \pm 4 \text{ Bq m}^{-2}$ ) and  
456 estimated the total global Pu (direct atmospheric deposition) in the ECS to be  $(1.3 \pm 0.1)$   
457  $\times 10^{13} \text{ Bq}$ . Using the arithmetic mean value of the  $^{239+240}\text{Pu}$  inventory in four segments  
458 of the ECS (details are shown in supplementary materials), the total buried Pu was  
459 estimated to be  $(3.1 \pm 1.4) \times 10^{13} \text{ Bq}$ . The PPG input was estimated to be  $(1.4 \pm 0.7)$   
460  $\times 10^{13} - (1.6 \pm 0.7) \times 10^{13} \text{ Bq}$  by total Pu  $\times$  Pu fraction of Pu derived from PPG.  
461 Moreover, the total inventory of the Yangtze input of  $^{239+240}\text{Pu}$  during 61 years  
462 (1952-2013) was estimated to be  $(0.15 \pm 0.08) \times 10^{13} \text{ Bq}$  based on the annual input  
463 rate from Yangtze River of  $(2.4 \pm 1.4) \times 10^{10} \text{ Bq}$ . Besides, we can observe that there  
464 was other source of Pu to the ECS with value of  $(0.06 \pm 0.05) \times 10^{13} - (0.28 \pm 0.24) \times$   
465  $10^{13} \text{ Bq}$ , characterized by the global fallout  $^{240}\text{Pu}/^{239}\text{Pu}$  atom ratio. Previous studies  
466 (Liu et al., 2003) had suggested that the finer part of sedimentary material of the  
467 Yellow River could be transported southward into the ECS, especially influenced by  
468 the strong southward coastal current during winter. Dai et al. (2011) reported that a  
469 small portion of sediment in the North Jiangsu coast could be transported into the  
470 north branch of the Yangtze River driven by the NJCC and then entered the ECS.  
471 Meanwhile, the  $^{240}\text{Pu}/^{239}\text{Pu}$  atom ratios in Lanzhou (the Yellow River catchment) and  
472 the North Jiangsu tidal flats were also reported to be  $\sim 0.18$  (Zheng et al., 2009; Liu et  
473 al., 2013). Considering all the observations above, we suggest that there is a small  
474 fraction of Pu that originated from the Yellow River and North Jiangsu coast that  
475 could be transported from the Yellow Sea to the ECS by the coastal currents. It is also  
476 anticipated that the contribution of the Yellow sea to the ECS will likely vary spatially  
477 within the ECS. Finally, we attempted to construct a mass balance (Fig. 7) of  
478 sedimentary  $^{239+240}\text{Pu}$  for sediment in the ECS. Although the Yangtze River input is  
479 the important Pu source for the estuary area of the Yangtze River, it is relatively small  
480 compared to the entire inventory of Pu in the ECS, and the dominant contribution of  
481  $^{239+240}\text{Pu}$  to the ECS remains from the PPG by the KC.

482 The TWC and the KC bring many nutrients to the ECS, with very volume of water  
483 of  $7.9 \times 10^{14} \text{ m}^3 \text{ y}^{-1}$  and  $4.1 \times 10^{13} \text{ m}^3 \text{ y}^{-1}$ , respectively (Kagimoto and Yamagata,

---

484 1997; Su, 2001). The mean  $^{239+240}\text{Pu}$  activity in the upper 200 m of sea water in the  
485 northeast of the Taiwan Island and near the KC was reported to be  $3.3\pm 2.7 \text{ mBq m}^{-3}$   
486 (CB-11; 25.24 °N, 124.52 °E; Nagaya and Nakamura, 1992), a value that is  
487 comparable to the decades mean value of surface water in the western Pacific Ocean  
488 ( $2.4 - 3.6 \text{ mBq m}^{-3}$ , Povinec et al., 2005). Using the mean  $^{239+240}\text{Pu}$  activity ( $3.3 \text{ mBq}$   
489  $\text{m}^{-3}$ ) and multiplying the total flow of the KC and TWC for 61 years (1952-2013), we  
490 can roughly estimate that  $(1.6\pm 1.3) \times 10^{14} \text{ Bq } ^{239+240}\text{Pu}$  passed through the ECS by the  
491 KC and TWC during the past six decades. Therefore, the buried  $^{239+240}\text{Pu}$  in sediments  
492 of ECS accounted for  $8.8\% \pm 8.3\% - 10.0\% \pm 9.2\%$  of the total  $^{239+240}\text{Pu}$  transported  
493 by the KC and TWC into the ECS. It should be noted that  $^{239+240}\text{Pu}$  concentration in  
494 the KC seawater might be much higher in 1950's than present; and these reported  
495 values in the seawater column might not include the particle associated Pu, so the  
496 estimation here might be a higher estimate. Considering the very high Pu contribution  
497 from the PPG input, the  $^{240}\text{Pu}/^{239}\text{Pu}$  atom ratio can not only be potentially used to  
498 obtain a better insight of the biogeochemistry influenced by the KC, but also used to  
499 trace the long-range transport of other particle-reactive radionuclides such as  $^{210}\text{Pb}$ ,  
500  $^{230}\text{Th}$ ,  $^{231}\text{Pa}$ , and other particle-reactive species.

## 501 5. Conclusion

502 Based on the Pu isotopic analysis and  $^{210}\text{Pb}_{\text{ex}}$  in the sediments of the ECS, the  
503 following conclusions are drawn:

504 The  $^{239, 240}\text{Pu}$  activity concentrations in the ECS surface sediments ranged  
505 between  $0.048$  and  $0.492 \text{ Bq kg}^{-1}$  (mean:  $0.188 \pm 0.007 \text{ Bq kg}^{-1}$ ). The  $^{240}\text{Pu}/^{239}\text{Pu}$  atom  
506 ratios in the ECS, ranging from  $0.158$  to  $0.297$  (mean:  $0.234 \pm 0.024$ ), exhibited a  
507 distribution pattern similar to that of the  $^{239, 240}\text{Pu}$  activities. The atom ratios were  
508 mostly higher than the global fallout value of  $0.18$  and were lower than the signature  
509 value ( $0.36$ ) of the PPG, which indicates an influence of PPG Pu input to the ECS.  
510 The sedimentation rates estimated from the penetration depths of  $^{239+240}\text{Pu}$  were  
511 similar to the values based on  $^{210}\text{Pb}_{\text{ex}}$  at cores E1, M7, B6, C12 and F8. Compared to  
512  $^{137}\text{Cs}$ ,  $^{239+240}\text{Pu}$  is a better time marker and can be used to calibrate the  $^{210}\text{Pb}_{\text{ex}}$   
513 chronology in marine environment.

514 The annual Yangtze River input of  $^{239+240}\text{Pu}$  is estimated to be  $2.4 \times 10^{10} \text{ Bq}$ ,  
515 which is small compared to the total Pu inventory of  $3.1 \times 10^{13} \text{ Bq}$  in the ECS shelf.  
516 However, the estimated  $^{239+240}\text{Pu}$  concentration in the suspended material in the  
517 Yangtze River ( $0.18 \text{ Bq kg}^{-1}$ ) is within the range of the values found in the Yangtze  
518 Estuary sediments, and the  $^{240}\text{Pu}/^{239}\text{Pu}$  atom ratios are  $\sim 0.18$ , which indicates that the



---

519 Yangtze River input dominates as the source of Pu in the estuary area in the ECS. The  
520 estimated PPG input of  $^{239+240}\text{Pu}$  is  $(1.4-1.6)\times 10^{13}$  Bq, which accounts for 45%-52%  
521 of the total Pu estimated in the entire ECS and the scavenging ratio of the total  
522  $^{239+240}\text{Pu}$  transported by the KC and TWC into ECS sediments is estimated to be  
523 ~10%. These Pu inputs were mainly deposited in coastal and shelf regions via  
524 scavenging process. Moreover, a small proportion of Pu could also have been  
525 transported from the Yellow Sea to the ECS by the coastal currents.  $^{240}\text{Pu}/^{239}\text{Pu}$  atom  
526 ratio can not only be potentially used to obtain a better insight of the biogeochemistry  
527 influenced by the KC, but also be used to trace the long-range transport of other  
528 particle-reactive radionuclides such as  $^{210}\text{Pb}$ ,  $^{230}\text{Th}$ ,  $^{231}\text{Pa}$ , and other particle-reactive  
529 organic and inorganic species that have similar  $K_d$ s as Pu.

530

### 531 **Acknowledgements**

532 This research was supported by the Ministry of Science and Technology of PR  
533 China (2011CB409801), the U.S. National Science Foundation (OCE-1237059), the  
534 China Scholarship Council (No. 201406140049) and the Fund of ECNU for Overseas  
535 Scholars. One of the authors, Mark Baskaran, is thankful for the support from the  
536 “*High-end Foreign Experts Recruitment Program*” sponsored by the State  
537 Administration of Foreign Affairs (P. R. China). We thank Editor, Dr. Martin Frank  
538 and two anonymous reviewers for their constructive comments for improvement of  
539 the original manuscript.

540

### 541 **References**

- 542 Baskaran, M., Asbill, S., Santschi, P., Brooks, J., Champ, M., Adkinson, D., Colmer,  
543 M. R., Makeyev, V., 1996. Pu,  $^{137}\text{Cs}$  and excess  $^{210}\text{Pb}$  in Russian Arctic sediments.  
544 Earth Planet. Sci. Lett. 140, 243–257.
- 545 Baskaran, M., Ravichandran M., Bianchi T. S., 1997. Cycling of  $^7\text{Be}$  and  $^{210}\text{Pb}$  in a  
546 high DOC, shallow, turbid estuary of southeast Texas. Estuarine Coastal Shelf Sci.  
547 45, 165-176.
- 548 Bu, W. T., Zheng, J., Guo, Q. J., Uchida, S., 2014. Vertical distribution and migration  
549 of global fallout Pu in forest soils in southwestern China. J. Environ. Radioact. 136,  
550 174–180.
- 551 Buesseler, K. O., 1997. The isotopic signature of fallout plutonium in the North  
552 Pacific. J. Environ. Radioact. 36, 69.
- 553 Buffoni, G., Delfanti, R., Papucci, C., 1992. Accumulation rates and mixing processes  
554 in near-surface North Atlantic sediments: Evidence from C-14 and Pu-239,240  
555 downcore profiles. Mar. Geol. 109 (1-2), 159-170.

- 
- 556 Che, Y., He, Q., Lin, W. Q., 2003. The distributions of particulate heavy metals and its  
557 indication to the transfer of sediments in the Changjiang Estuary and Hangzhou  
558 Bay, China. *Mar. Pollut. Bull.* 46(1), 123-131.
- 559 China Water Resources Committee (CWRC), 2013. China River Sediment Bulletin.  
560 Ministry of Water Resources of China (ed.) China Water Power Press, Beijing (in  
561 Chinese).
- 562 Clark, M. J., Smith, F. B., 1988. Wet and dry deposition of Chernobyl releases. *Nature*  
563 332, 245 – 249.
- 564 Cochran, J. K., Hirschberg, D. J., Livingston, H. D., Buesseler, K. O., Key, R. M.,  
565 1995. Natural and anthropogenic radionuclide distributions in the Nansen  
566 Catchment, Arctic Ocean: Scavenging rates and circulation timescales. *Deep Sea*  
567 *Res. Part II*, 42, 1495–1517.
- 568 Dai, Z. J., Du, J. Z., Chu, A., Zhang, X. L., 2011. Sediment characteristics in the  
569 North Branch of the Yangtze Estuary based on radioisotope tracers. *Environ. Earth*  
570 *Sci.* 62(8), 1629-1634.
- 571 Dai, Z. J., Liu, J. T., 2013. Impacts of large dams on downstream fluvial  
572 sedimentation: an example of the Three Gorges Dam (TGD) on the Changjiang  
573 (Yangtze River). *J. Hydrol.* 480, 10-18.
- 574 Dai, Z., Liu, J., Wei, W., Chen J., 2014. Detection of the Three Gorges Dam influence  
575 on the Changjiang (Yangtze River) submerged delta. *Sci. Rep.* 4, 6600,  
576 doi:10.1038/srep06600.
- 577 DeMaster, D. J., Kuehl, S. A., Nittrouer, C. A., 1986. Effects of suspended sediments  
578 on geochemical processes near the mouth of the Amazon River: examination of  
579 biological silica uptake and the fate of particle-reactive elements. *Cont. Shelf Res.*  
580 6, 107– 125.
- 581 Delfanti, R., Klein, B., Papucci, C., 2003. Distribution of <sup>137</sup>Cs and other radioactive  
582 tracers in the eastern Mediterranean: Relationship to the deepwater transient. *J.*  
583 *Geophys. Res.* 108(C9), 8108, doi:10.1029/2002JC001371.
- 584 Dominik, J., Burrus, D. Vernet, J. P., 1987. Transport of the environmental  
585 radionuclides in an alpine watershed. *Earth Planet. Sci. Lett.* 84, 165–180.
- 586 Donaldson L. R., Seymour A. H., Nevissi A. E., 1997. University of Washington's  
587 radioecological studies in the Marshall Islands, 1946–1997. *Health Physics* 73, 214  
588 – 222.
- 589 Dong, W., Tims, S. G., Fifield, L. K., Guo, Q. J., 2010. Concentration and  
590 characterization of plutonium in soils of Hubei in central China. *J. Environ.*  
591 *Radioact.* 101, 29–32.
- 592 Dou, Y., Yang, S., Liu, Z., Clift, P. D., Shi, X., Yu, H. Berne, S., 2010. Provenance  
593 discrimination of siliciclastic sediments in the middle Okinawa Trough since 30 ka:  
594 Constraints from rare earth element compositions. *Mar. Geol.* 275(1), 212-220.
- 595 Du, J., Wu, Y., Huang, D., Zhang, J., 2010, Use of <sup>7</sup>Be, <sup>210</sup>Pb and <sup>137</sup>Cs tracers to the  
596 transport of surface sediments of the Changjiang Estuary, China, *J. Mar. Syst.* 82  
597 (4), 286–294.
- 598 Hamilton, T. F., 2004. Linking legacies of the cold war to arrival of anthropogenic  
599 radionuclides in the oceans through the 20th century. *Marine radioactivity* 6, 30-87.
- 600 Hu, D., Wu, L., Cai, W., Gupta, A. S., Ganachaud, A., Qiu, B., Gordon, A. L., Lin, X.,  
601 Chen, Z., Hu, S., Wang, G., Wang, Q., Sprintall, J., Qu, T., Kashino, Y., Wang, F.,

- 
- 602 Kessler, W., 2015. Pacific western boundary currents and their roles in climate.  
603 Nature 522(7556), 299-308.
- 604 Huang, D., Du, J., Moore, W. S., Zhang, J. 2013. Particle dynamics of the Changjiang  
605 Estuary and adjacent coastal region determined by natural particle - reactive  
606 radionuclides ( $^7\text{Be}$ ,  $^{210}\text{Pb}$ , and  $^{234}\text{Th}$ ). J. Geophys. Res. Oceans 118(4), 1736-1748.
- 607 Huh, C. A., Su, C. C., 1999. Sedimentation dynamics in the East China Sea elucidated  
608 from  $^{210}\text{Pb}$ ,  $^{137}\text{Cs}$ , and  $^{239,240}\text{Pu}$ . Mar. Geol. 160,183–196.
- 609 Kagimoto, T., Yamagata, T., 1997. Seasonal transport variations of the Kuroshio: An  
610 OGCM simulation. J. Phys. Oceanogr. 27(3), 403-418.
- 611 Kelley, J. M., Bond, L. A., Beasley, T. M., 1999. Global distribution of Pu isotopes  
612 and  $^{237}\text{Np}$ . Sci. Total Environ. 237/238, 483–500.
- 613 Kersting, A. B., Efurud, D. W., Finnegan, D. L., Rokop, D. J., Smith, D. K.,  
614 Thompson, J. L., 1999. Migration of plutonium in ground water at the Nevada Test  
615 Site. Nature 397(6714), 56-59.
- 616 Kim C. K., Kim C. S., Chang B. U., Choi S.W., Chung C. S., Hong G. H., Hirose, H.,  
617 Igarashi, Y., 2004. Plutonium isotopes in seas around the Korean Peninsula. Sci.  
618 Total Environ. 318, 197 – 209.
- 619 Krey, P. W., Hardy, E. P., Pachucki, C., Rourke, F., Coluzza, J., Benson, W. K., 1976.  
620 Mass isotopic composition of global fallout plutonium in soil. Transuranium  
621 Nuclides in the Environment (Proceedings Series); IAEA: Vienna, pp 671 –678.
- 622 Lee, S. Y., Huh, C. A., Su, C. C., You, C. F., 2004. Sedimentation in the Southern  
623 Okinawa Trough: enhanced particle scavenging and teleconnection between the  
624 Equatorial Pacific and western Pacific margins. Deep Sea Res. Part I:  
625 Oceanographic Research Papers, 51(11), 1769-1780.
- 626 Li, Z. Q., Wu, Y., Liu S. M., Du, J. Z., Zhang, J., 2015. An 800-year record of  
627 terrestrial organic matter from the East China Sea shelf break: Links to climate  
628 change and human activity in the Changjiang Catchment. Deep-Sea Res. II. 113,  
629 1-10.
- 630 Liao, H., Zheng, J., Wu, F., Yamada, M., Tan, M., Chen, J., 2008. Determination of  
631 plutonium isotopes in freshwater lake sediments by sector-field ICP-MS after  
632 separation using ion-exchange chromatography. Appl. Radio. Isot. 66(8),  
633 1138-1145.
- 634 Lindahl, P., Asami, R., Iryu, Y., Worsfold, P., Keith-Roach, M., Choi, M. S., 2011.  
635 Sources of plutonium to the tropical Northwest Pacific Ocean (1943–1999)  
636 identified using a natural coral archive. Geochim. Cosmochim. Acta 75(5),  
637 1346-1356.
- 638 Liu, J. P, Li, A. C., Xu, K. H., Velozzi, D. M., Yang, Z. S, Milliman, J. D., DeMaster,  
639 D. J., 2006. Sedimentary features of the Changjiang River-derived along-shelf  
640 clinoform deposit in the East China Sea. Cont. Shelf Res. 26, 2141-2156.
- 641 Liu, J., Zhu, R. X., Li, G. X., 2003. Rock magnetic properties of the fine grained  
642 sediment on the outer shelf of the East China Sea: implication for provenance. Mar.  
643 Geol. 193,195– 206.
- 644 Liu, S., Zhang, W., He, Q., Li, D., Liu, H. Yu, L., 2010. Magnetic properties of East  
645 China Sea shelf sediments off the Yangtze Estuary: Influence of provenance and  
646 particle size. Geomorphology 119(3), 212-220.
- 647 Liu, Z. Y., Zheng J., Pan S., Dong W., Yamada M., Aono, T., Guo Q., 2011. Pu and

---

648 <sup>137</sup>Cs in the Yangtze River Estuary sediments: Distribution and Source  
649 Identification. *Environ. Sci. Technol.* 45 (5), 1805-1811.

650 Liu, Z. Y., Zheng, J., Pan, S. M., Gao, J. H., 2013. Anthropogenic plutonium in the  
651 North Jiangsu tidal flats of the Yellow Sea in China. *Environ Monit Assess.* 185,  
652 6539–6551.

653 McKee, B.A., Nittrouer, C.A., DeMaster, D.J., 1983. The concepts of sediment  
654 deposition and accumulation applied to the continental shelf near the mouth of the  
655 Changjiang River. *Geology* 11, 631– 633.

656 Moon, D., Hong, G., Kim, Y.I., Baskaran, M., Chung, C.S., Kim, S.H., 2003.  
657 Accumulation of anthropogenic and natural radionuclides in bottom sediments of  
658 the Northwest Pacific Ocean. *Deep-Sea Res. Part II: Topical Studies in*  
659 *Oceanography* 50 (17-21), 2649-2673.

660 Muramatsu, Y., Uchida S., Tagami K., Yoshida, S., Fujikawa, T., 1999.  
661 Determination of plutonium concentration and its isotopic ratio in environmental  
662 materials by ICP-MS after separation using and extraction chromatography. *J. Anal.*  
663 *Atom. Spectrom.* 14(5), 859-865.

664 Muramatsu, Y., Hamilton, T., Uchida, S., Tagami, K., Yoshida, S., Robison, W., 2001.  
665 Measurement of <sup>240</sup>Pu/<sup>239</sup>Pu isotopic ratios in soils from the Marshall Islands using  
666 ICP-MS. *Sci. Total Environ.* 278(1), 151-159.

667 Nagaya, Y., Nakamura, K., 1992. <sup>239,240</sup>Pu and <sup>137</sup>Cs in the east China and the Yellow  
668 seas. *J. Oceanogr.* 48, 23–35.

669 Olsen, C.R., Thein, M., Larsen, I. L., Lowry, P. D., Mulholland, P. J., Cutshall, N. H.,  
670 Byrd, J. T., Windom, H. L., 1989. Plutonium, lead-210, and carbon isotopes in the  
671 Savannah estuary: riverborne versus marine sources. *Environ. Sci. Technol.* 23,  
672 1475-1481.

673 Oguri, K., Matsumoto, E., Yamada, M., Saito, Y., Iseki, K., 2003. Sediment  
674 accumulation rates and budgets of depositing particles of the East China Sea. *Deep*  
675 *Sea Res. Part II: Topical Studies in Oceanography* 50(2), 513-528.

676 Pan, S. M., Tims, S. G., Liu, X. Y., Fifield, L. K., 2011. <sup>137</sup>Cs, <sup>239+240</sup>Pu  
677 concentrations and the <sup>240</sup>Pu/<sup>239</sup>Pu atom ratio in a sediment core from the  
678 sub-aqueous delta of Yangtze River estuary. *J. Environ. Radioact.* 102(10),  
679 930-936.

680 Peirson, D. H., Cambray, R. S., Cawse, P. A., Eakins, J. D., Pattenden, N. J., 1982.  
681 Environmental radioactivity in Cumbria. *Nature* 300, 27-32.

682 Povinec, P.P., Livingston, H.D., Shima, S., Aoyama, M., Gastaud, J., Goroncy, I.,  
683 Hirose, K., Huynh-Ngoc, L., Ikeuchi, Y., Ito, T., La Rosa, J., Kwong, L.L.W., Lee,  
684 S.H., Moriya, H., Mulsow, S., Oregioni, B., Pettersson, H., Togawa, O., 2003.  
685 IAEA'97 expedition to the NW Pacific Ocean-results of oceanographic and  
686 radionuclide investigations of the water column. *Deep-Sea Res. II* 50, 2607–2637.

687 Povinec, P. P., Aarkrog, A., Buesseler, K. O., Delfanti, R., Hirose, K., Hong, G. H.,  
688 Ito, T., Livingston, H. D., Niles, H., Noshkin, V. E., Shima, S., Togawa, O., 2005.  
689 <sup>90</sup>Sr, <sup>137</sup>Cs and <sup>239,240</sup>Pu concentration surface water time series in the Pacific and  
690 Indian Oceans–WOMARS results. *J. Environ. Radioact.* 81(1), 63-87.

691 Qiao, J., Shi, K., Hou, X., Nielsen, S., Roos, P., 2014. Rapid multisample analysis for  
692 simultaneous determination of anthropogenic radionuclides in marine environment.  
693 *Environ. Sci. Technol.* 48(7), 3935-3942.

694 Ravichandran, M., Baskaran, M., Santschi, P. H., Bianchi, T. S., 1995.  
695 Geochronology of sediments in the Sabine-Neches estuary, Texas, USA. *Chem.*

---

696 Geol. 125, 291-306.

697 Santschi, P. H., Li, Y. H., Bell, J. J., Trier, R. M., Kawtaluk, K., 1980. Pu in coastal  
698 marine environment. *Earth Planet. Sci. Lett.* 51, 248-265.

699 Scott, M. R., Rotter, R. J., Salter, P. F., 1985. Transport of fallout plutonium to the  
700 ocean by the Mississippi River. *Earth Planet. Sci. Lett.* 75(4), 321-326.

701 Smith, J. N., Ellis, K. M., Nelson, D. M., 1987. Time-dependent modeling of fallout  
702 radionuclide transport in a drainage catchment: significance "of slow" erosional and  
703 fast hydrological components. *Chem. Geol.* 63, 157-180.

704 Su, C. C., Huh, C. A., 2002.  $^{210}\text{Pb}$ ,  $^{137}\text{Cs}$  and  $^{239;240}\text{Pu}$  in East China Sea sediments:  
705 sources, pathways and budgets of sediments and radionuclides. *Mar. Geol.* 183,  
706 163-178.

707 Su, J. L. 2001. A review of circulation dynamics of the coastal oceans near China (in  
708 Chinese with English abstract). *Acta Oceanol. Sin.* 23(4), 1-16.

709 UNSCEAR, United Nations Scientific Committee on the Effects of Atomic Radiation  
710 Exposures to the Public from Man-made Sources of Radiation, Sources and Effects  
711 of Ionizing Radiation, United Nations, New York, 2000, 654 pp.

712 Wang, J., Du, J., Baskaran, M., Zhang, J., 2016. Mobile mud dynamics in the East  
713 China Sea elucidated using  $^{210}\text{Pb}$ ,  $^{137}\text{Cs}$ ,  $^7\text{Be}$ , and  $^{234}\text{Th}$  as tracers, *J. Geophys. Res.*  
714 *Oceans* 121, 224-239.

715 Wang, Z. L., Yamada, M., 2005. Plutonium activities and  $^{240}\text{Pu}/^{239}\text{Pu}$  atom ratios in  
716 sediment cores from the East China Sea and Okinawa Trough: Sources and  
717 inventories. *Earth Planet. Sci. Lett.* 233, 441-453.

718 Wu, F., Zheng, J., Liao, H., Yamada, M., 2010. Vertical distributions of plutonium and  
719  $^{137}\text{Cs}$  in lacustrine sediments in northwestern China: quantifying sediment  
720 accumulation rates and source identifications. *Environ. Sci. Technol.* 44(8),  
721 2911-2917.

722 Wu, H., 2015. Cross-shelf penetrating fronts: A response of buoyant coastal water to  
723 ambient pycnocline undulation. *J. Geophys. Res. Oceans* 120(7), 5101-5119.

724 Wu, J., Zheng, J., Dai, M., Huh, C. A., Chen, W., Tagami, K., Uchida, C., 2014.  
725 Isotopic Composition and Distribution of Plutonium in Northern South China Sea  
726 Sediments Revealed Continuous Release and Transport of Pu from the Marshall  
727 Islands. *Environ. Sci. Technol.* 48, 3136-3144.

728 Xu, Y., Qiao, J., Hou, X., Pan, S., Roos, P., 2014. Determination of plutonium  
729 isotopes ( $^{238}\text{Pu}$ ,  $^{239}\text{Pu}$ ,  $^{240}\text{Pu}$ ,  $^{241}\text{Pu}$ ) in environmental samples using radiochemical  
730 separation combined with radiometric and mass spectrometric measurements.  
731 *Talanta* 119, 590-595.

732 Yamada, M., Zheng, J., Wang, Z. L., 2006.  $^{137}\text{Cs}$ ,  $^{239+240}\text{Pu}$  and  $^{240}\text{Pu}/^{239}\text{Pu}$  atom  
733 ratios in the surface waters of the western North Pacific Ocean, eastern Indian  
734 Ocean and their adjacent seas. *Sci. Total Environ.* 366(1), 242-252.

735 Yang, S. L., Milliman, J. D., Li, P., Xu, K., 2011. 50,000 dams later: erosion of the Yangtze  
736 River and its delta. *Global Planet. Change* 75(1), 14-20.

737 Zhao, C., Qiao, F. L., Wang, G. S., Xia, C. S., Jung, K. T., 2014. Simulation and  
738 prediction of  $^{137}\text{Cs}$  from the Fukushima accident in the China Seas. *Science China.*  
739 (34), 3416-3423.

740 Zheng, J., Yamada, M., 2004. Sediment core record of global fallout and Bikini  
741 closein fallout Pu in Sagami Bay, Western Northwest Pacific Margin. *Environ. Sci.*

- 
- 742 Technol. 38, 3498-3504.
- 743 Zheng, J., Yamada, M. 2006. Plutonium isotopes in settling particles: transport and  
744 scavenging of Pu in the western Northwest Pacific. *Environ. Sci. Technol.* 40(13),  
745 4103-4108.
- 746 Zheng, J., Yamada, M., Wu, F. C., Liao, H. Q., 2009. Characterization of Pu  
747 concentration and its isotopic composition in soils of Gansu in the northwestern  
748 China. *J. Environ. Radioact.* 100, 71-75.
- 749 Zheng, J., Aono, T., Uchida, S., Zhang, J., Honda, M. C., 2012. Distribution of Pu  
750 isotopes in marine sediments in the Pacific 30 km off Fukushima after the  
751 Fukushima Daiichi nuclear power plant accident. *Geochem. J.*, 46(4), 361-369.

---

752 **Figure Captions**

753 Figure 1 Location of sites occupied during the August cruise tracts in 2013 (surface  
754 sediment in blue and sediment core in purple). Several sediment cores from  
755 literature are marked in red color (6, BC16, Su and Huh, 2002; 18, Liu et al., 2011;  
756 SC07, Pan et al., 2011). Bathymetry (m) of the ECS shelf is also shown by  
757 grey lines. The summer regional surface currents are modified after Su,  
758 2001 and Hu et al., 2015: Changjiang diluted water (CDW, Summer);  
759 Zhejiang-Fujian Coast Current (ZFCC, Winter); North Jiangsu Coast  
760 Current (NJCC); Yellow Sea Coastal Current (YSCC); Yellow Sea Warm  
761 Current (YSWC); Taiwan Warm Current (TWC); Kuroshio Current (KC);  
762 North Equatorial Current (NEC); Mindanao Current (MC). Several rivers  
763 are also plotted, including a: Yellow River (5460 km), b: Yangtze River  
764 (6400 km), c: Qiantang River (589 km), d: Jiao River (206 km), e: Ou  
765 River (384 km), f: Min River (562 km).

766 Figure 2 Spatial distribution of the  $^{239}\text{Pu}$ ,  $^{240}\text{Pu}$ ,  $^{239+240}\text{Pu}$  activities and  $^{240}\text{Pu}/^{239}\text{Pu}$   
767 atom ratios of surface sediment in August of 2013.

768 Figure 3 The synthesis of  $^{240}\text{Pu}/^{239}\text{Pu}$  atom ratios in the areas surrounding the ECS:  
769 Chinese and Japanese soil (black color, Muramatsu et al., 1999, 2003;  
770 Zheng et al., 2009; Dong et al., 2010; Liu et al., 2013; Bu et al., 2014),  
771 sediment (red color, This study; Buesseler, 1997; Zheng and Yamada,  
772 2004; Wang and Yamada, 2005; Liu et al., 2011; Wu et al., 2014),  
773 seawater (blue color, Kim et al., 2004; Yamada et al., 2006) and a natural  
774 coral (orange color, Lindahl et al., 2011).

775 Figure 4 Distribution of  $\text{In}(^{210}\text{Pb}_{\text{ex}})$  and  $^{137}\text{Cs}$  activities in sediment cores collected  
776 from the ECS at six stations: estuary (C1), South inshore (E1), North  
777 offshore (M7, B7), and Okinawa trough (C12, F8).

778 Figure 5  $^{239+240}\text{Pu}$ , and  $^{240}\text{Pu}/^{239}\text{Pu}$  atom ratios in sediment cores collected from the  
779 ECS at six stations.

780 Figure 6 Spatial distribution of  $^{239+240}\text{Pu}$  inventories in sediment, including literature  
781 datas (Nagaya and Nakamura, 1992; Su and Huh, 1999; 2002; Wang and  
782 Yamada, 2005; Pan et al., 2011; Liu et al., 2011).

783 Figure 7 The mass balance of  $^{239+240}\text{Pu}$  in sediment in the ECS.

Fig 1

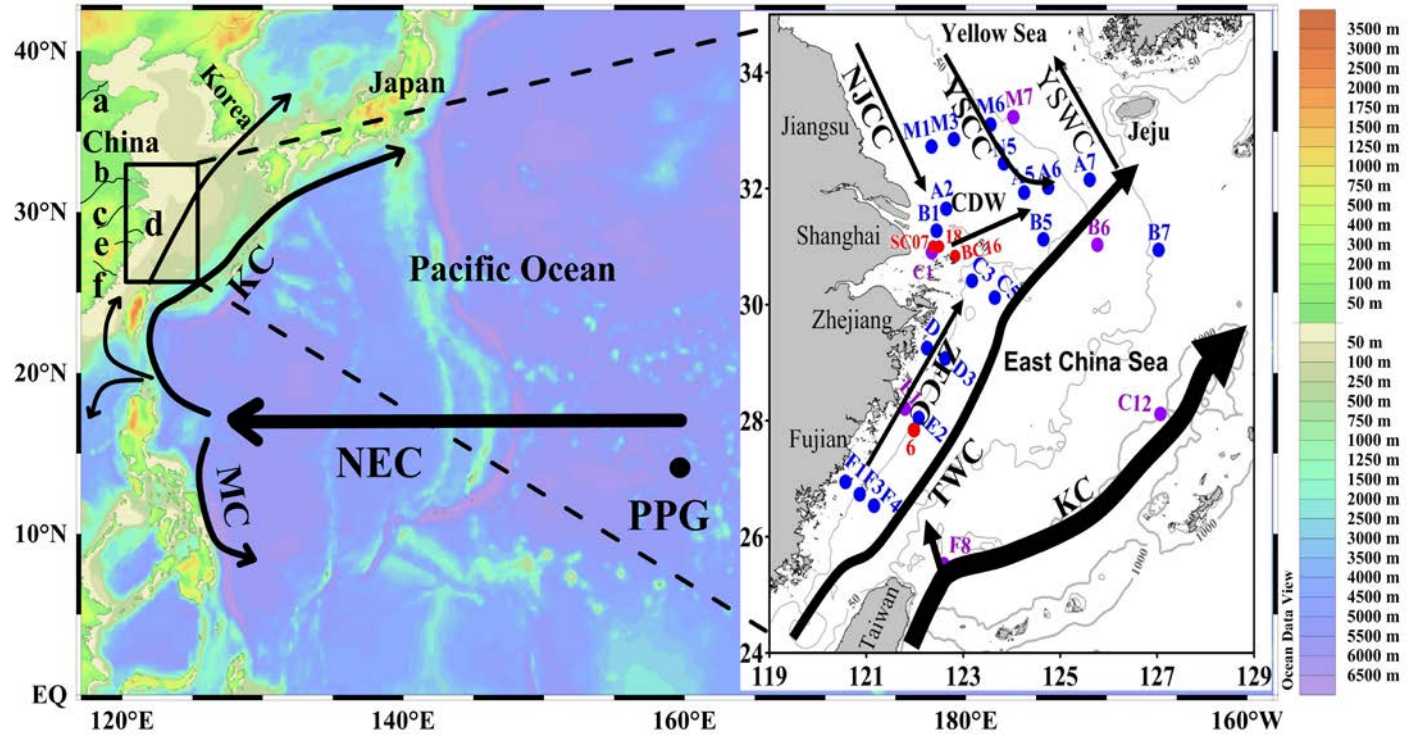




Fig 2

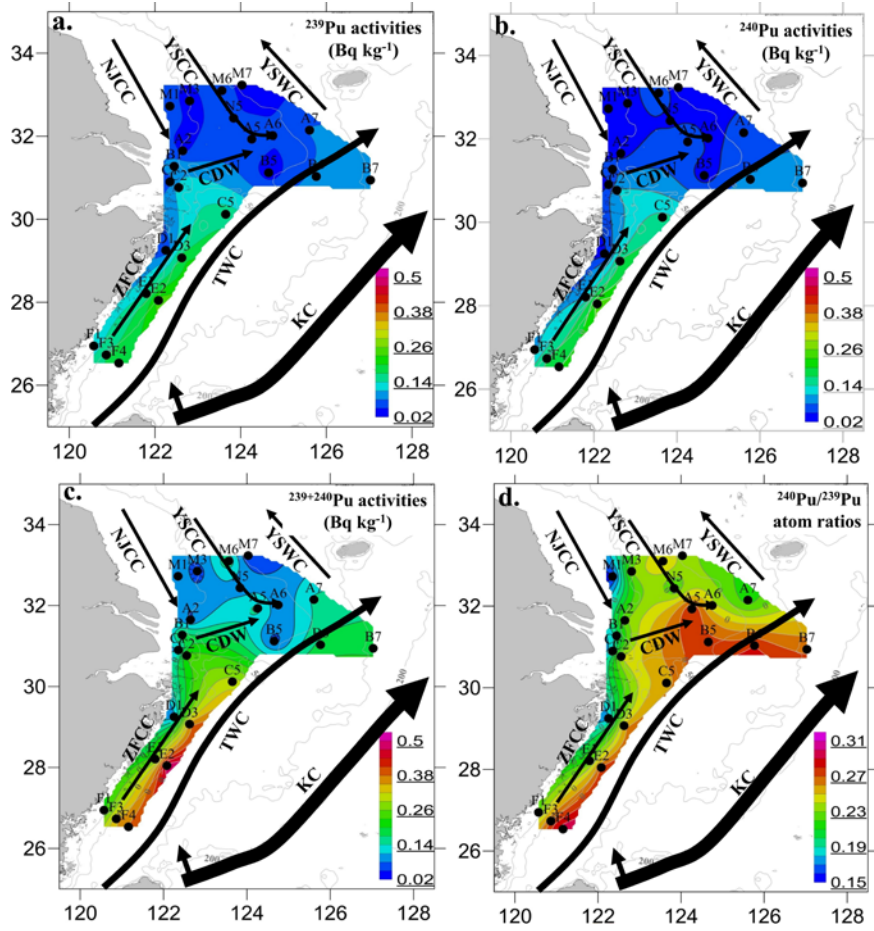


Fig 3

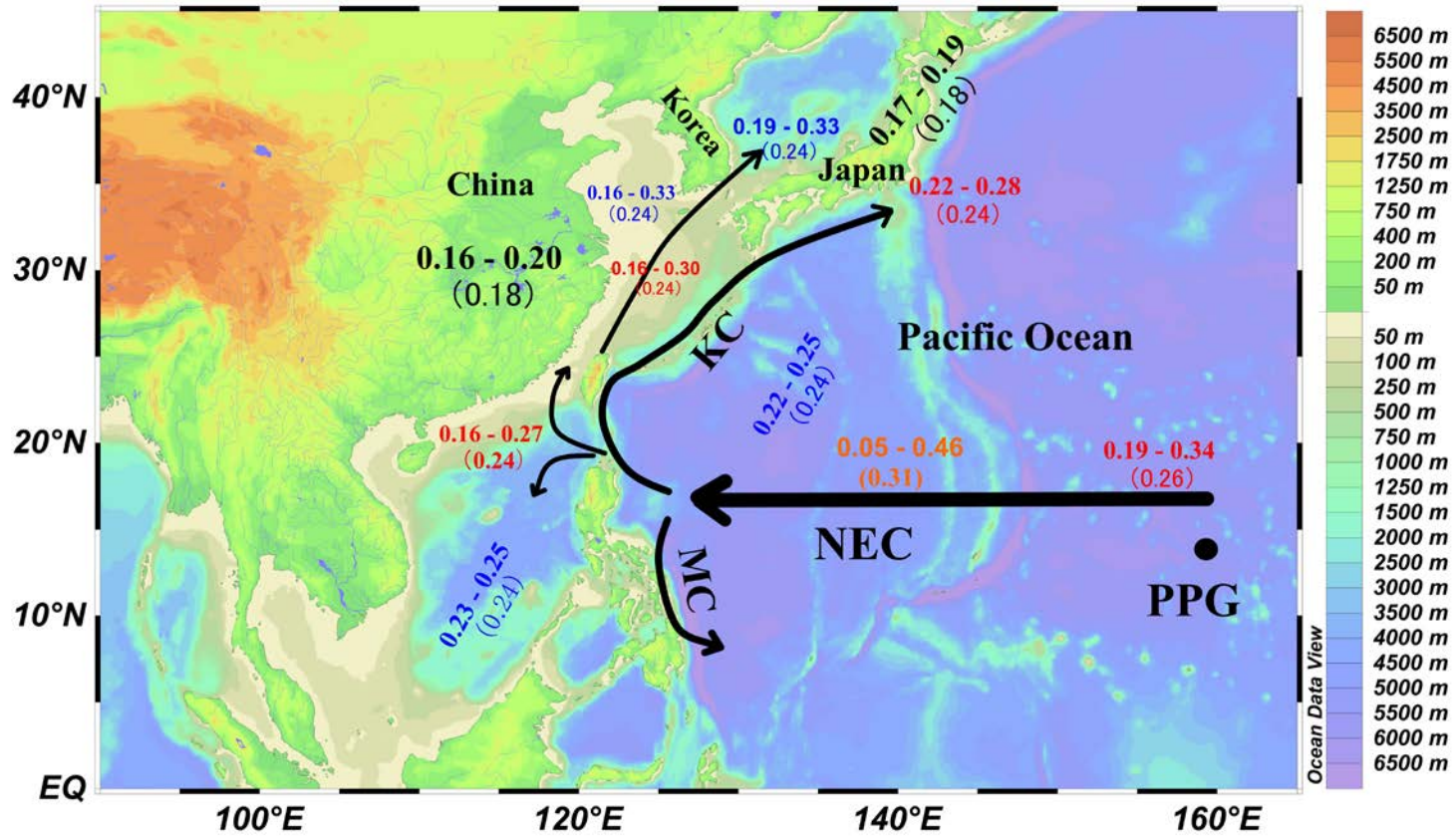


Fig 4

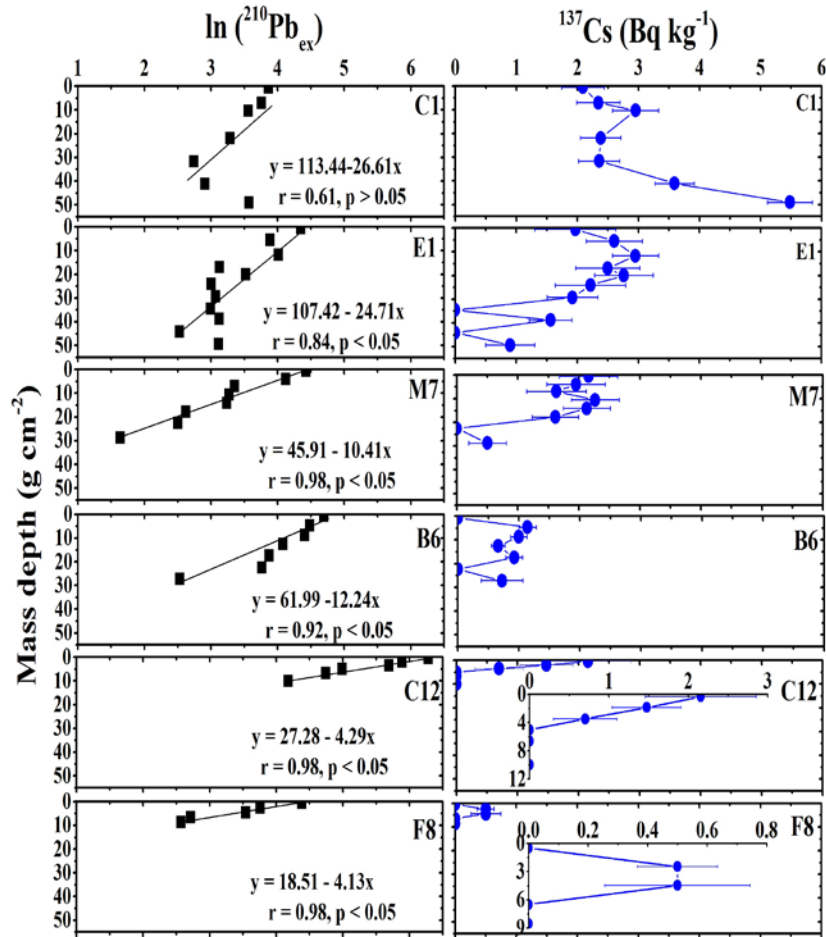


Fig 5

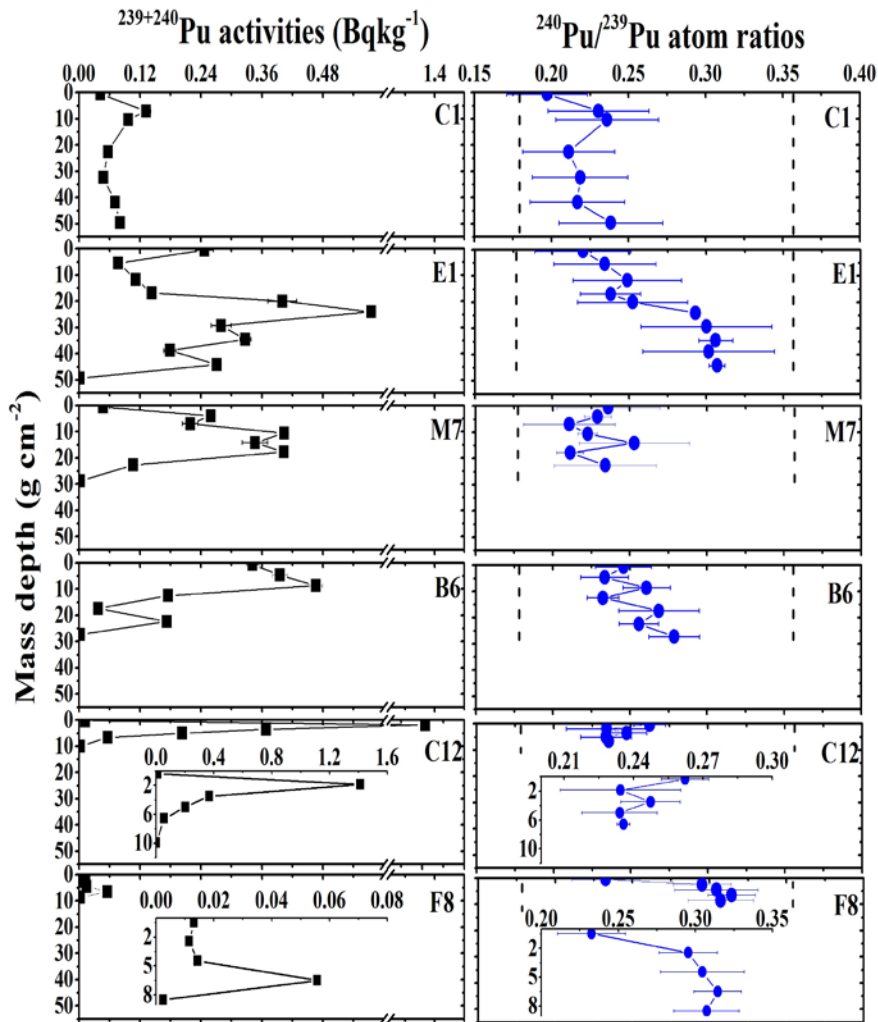




Fig 7

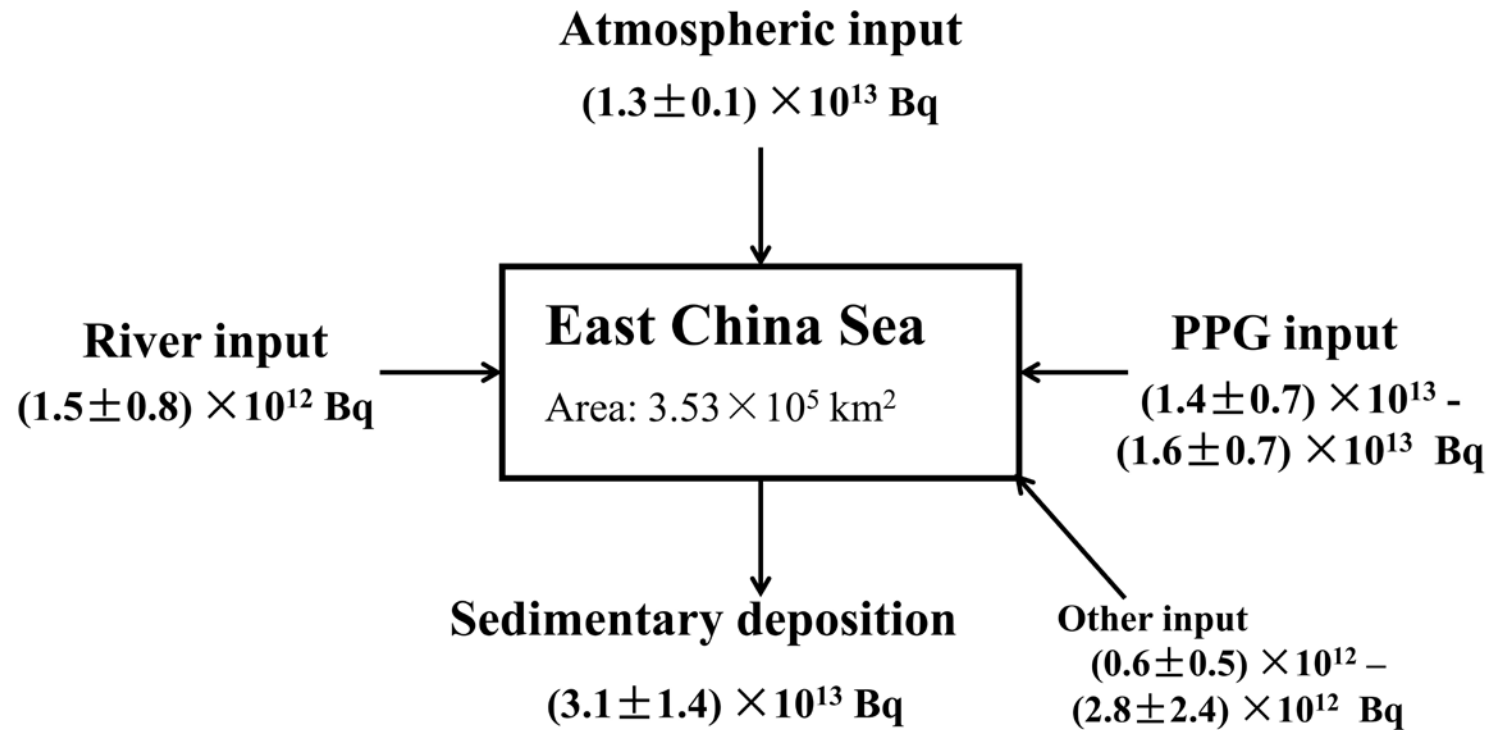


Table 1

Inventories of  $^{239}\text{Pu}$ ,  $^{240}\text{Pu}$ ,  $^{239+240}\text{Pu}$  and the mean  $^{240}\text{Pu}/^{239}\text{Pu}$  atom ratios in sediment cores from the ECS.

| Sample      | Longitude (E) | Latitude (N) | Water depth (m) | $^{239+240}\text{Pu}$ (Bq m <sup>-2</sup> ) | $^{240}\text{Pu}/^{239}\text{Pu}$ | $^{239}\text{Pu}$ (Bq m <sup>-2</sup> ) | $^{240}\text{Pu}$ (Bq m <sup>-2</sup> ) | References                |                  |
|-------------|---------------|--------------|-----------------|---|-----------------------------------|---|---|---------------------------|------------------|
| Estuary     | 122-124       | 30-32        | 23-58 (42)      | 48.5-807 (245)                              |                                   |   |   |                           |                  |
| Inner shelf | 120-124       | 26-30        | 26-84 (55)      | 81.7-420 (221)                              |                                   |   |   | Su and Huh, 2002          |                  |
| Outer shelf | 122.124.5     | 26-32        | 55-67 (61)      | 50.1-117 (83.3)                             |                                   |   |   |                           |                  |
| Slope       | 124.5-125     | 28.5-29.5    | 232-1053 (735)  | 16.7-93.3 (43.7)                            |                                   |   |   |                           |                  |
| CB-7-2      | 125.37        | 25.78        | 2170            | 8.9 ± 0.3                                   |                                   |   |   |                           |                  |
| CB17        | 123.50        | 28.50        | 65              | 79.9 ± 2.2                                  | No data reported                  |   |   | Nagaya and Nakamura, 1992 |                  |
| CB23        | 123.51        | 32.50        | 42              | 77.4 ± 1.4                                  |                                   |   |   |                           |                  |
| CB34        | 123.50        | 33.00        | 37              | 53.8 ± 1.3                                  |                                   |   |   |                           |                  |
| CB35        | 123.50        | 33.50        | 64              | 16.2 ± 0.3                                  |                                   |   |   |                           |                  |
| G2          | 126.74        | 28.00        | 999             | 32.5 ± 2.3                                  | 0.245** ± 0.017                   | 17.1 ± 1.2                              | 15.4 ± 1.1                              |                           |                  |
| PN3*        | 127.35        | 28.10        | 1000            | 47.2 ± 3.1                                  | 0.258** ± 0.018                   | 24.2 ± 2.3                              | 23.0 ± 1.1                              | Wang and Yamada, 2005     |                  |
| SST1*       | 127.38        | 28.38        | 1080            | 47.0 ± 2.3                                  | 0.230** ± 0.012                   | 25.5 ± 1.2                              | 21.5 ± 1.2                              |                           |                  |
| PN5*        | 126.43        | 28.80        | 127             | 101 ± 5.2                                   | 0.263** ± 0.014                   | 51.2 ± 3.2                              | 49.5 ± 2.1                              |                           |                  |
| PN8*        | 125.09        | 29.59        | 87              | 60.9 ± 4.4                                  | 0.254** ± 0.016                   | 31.5 ± 2.3                              | 29.4 ± 1.6                              |                           |                  |
| PN12*       | 123.08        | 31.20        | 50              | 81.5 ± 3.6                                  | 0.242** ± 0.010                   | 43.2 ± 2.1                              | 38.3 ± 1.5                              |                           |                  |
| C1          | 122.35        | 30.90        | 13              | 35.6 ± 2.5                                  | 0.221 ± 0.014                     | 19.6 ± 2.0                              | 16.0 ± 1.6                              |                           |                  |
| E1          | 121.80        | 28.21        | 22              | 118 ± 5.0                                   | 0.270 ± 0.034                     | 58.3 ± 3.3                              | 59.6 ± 3.7                              | This study                |                  |
| M7          | 124.03        | 33.23        | 66              | 65.4 ± 2.5                                  | 0.228 ± 0.015                     | 35.8 ± 1.7                              | 29.5 ± 1.8                              |                           |                  |
| B6          | 125.77        | 31.03        | 62              | 58.3 ± 4.6                                  | 0.254 ± 0.018                     | 30.7 ± 2.6                              | 27.7 ± 3.7                              |                           |                  |
| C12         | 127.07        | 28.12        | 998             | 33.9 ± 0.7                                  | 0.243 ± 0.012                     | 18.2 ± 0.4                              | 15.7 ± 0.6                              |                           |                  |
| F8          | 122.60        | 25.53        | 619             | 1.9 ± 0.1                                   | 0.291 ± 0.033                     | 0.9 ± 0.0                               | 1.0 ± 0.0                               |                           |                  |
| SC07*       | 122.38        | 31.00        | 14              | 407 ± 27.0                                  | 0.242** ± 0.023                   | 215.7 ± 24.9                            | 191.3 ± 30.9                            |                           | Pan et al., 2011 |
| 18*         | 122.50        | 31.00        | 20              | 388 ± 21.0                                  | 0.237** ± 0.011                   | 207.6 ± 20.2                            | 180.4 ± 17.9                            |                           | Liu et al., 2011 |

**Kommenterede [XH1]:** The uncertainty cannot be 0.0. For example, it can be presented as 0.92±0.04, and 1.04±0.04

---

\*: The Pu inventories ( $^{239+240}\text{Pu}$ ) were calculated as follows: total inventory of  $^{239+240}\text{Pu}$  in each layer = (mass depth in that layer  $\times$  ( $^{239}\text{Pu}$  activity +  $^{240}\text{Pu}$  activity in that layer); total  $^{239+240}\text{Pu}$  inventory = summation of inventory in each layer; for all other samples, the total Pu were measured by alpha spectrometry which is a measure of the combined activity of  $^{239}\text{Pu}$  and  $^{240}\text{Pu}$ , as alpha spectrometry method yields  $^{239,240}\text{Pu}$  activity due to overlapping alpha energies of  $^{239}\text{Pu}$  and  $^{240}\text{Pu}$ .

\*\* : The mean  $^{240}\text{Pu}/^{239}\text{Pu}$  atom ratios were calculated as follows: the total inventory of  $^{239+240}\text{Pu}$   $\times$  the  $^{240}\text{Pu}/^{239}\text{Pu}$  ratio in each layer / the sum of  $^{239+240}\text{Pu}$  inventory in each layer.



Table 2

Inventories of  $^{239}\text{Pu}$ ,  $^{240}\text{Pu}$ ,  $^{239+240}\text{Pu}$  and the mean  $^{240}\text{Pu}/^{239}\text{Pu}$  atom ratios in sediment cores from the Yangtze River catchment.

| Sample           | Longitude<br>(E) | Latitude<br>(N) | $^{239+240}\text{Pu}$<br>(Bq m <sup>-2</sup> ) | $^{240}\text{Pu}/^{239}\text{Pu}$ | $^{239}\text{Pu}$<br>(Bq m <sup>-2</sup> ) | $^{240}\text{Pu}$<br>(Bq m <sup>-2</sup> ) | References                           |
|------------------|------------------|-----------------|--|-----------------------------------|--|--|--------------------------------------|
| Southwest China  |                  |                 |  |                                   |  |  |                                      |
| GY*              | 106.67           | 26.66           | 63.0 ± 2.4                                     | 0.191** ± 0.010                   | 37.0 ± 2.3                                 | 26.0 ± 2.3                                 |                                      |
| WL*              | 107.85           | 29.52           | 114.0 ± 5.9                                    | 0.185** ± 0.004                   | 67.9 ± 5.8                                 | 46.1 ± 3.4                                 | Bu et al., 2014                      |
| ZX*              | 107.85           | 30.53           | 19.0 ± 1.6                                     | 0.182** ± 0.008                   | 11.4 ± 1.6                                 | 7.6 ± 1.0                                  |                                      |
| Central China    |                  |                 |  |                                   |  |  |                                      |
| DK*              | 112.19           | 31.15           | 44.9 ± 5.9                                     | 0.183** ± 0.052                   | 26.9 ± 5.0                                 | 18.0 ± 7.5                                 | Dong et al., 2010                    |
| GLZ*             | 111.42           | 32.24           | 54.6 ± 4.4                                     | 0.200** ± 0.013                   | 31.5 ± 4.2                                 | 23.1 ± 3.4                                 |                                      |
| Atmospheric fall |                  | 20-30           | 36.0   | 0.180                             | 21.7                                       | 14.3                                       | Kelley et al. 1999;<br>UNSCEAR, 2000 |
|                  |                  | 30-40           | 42.0   |                                   | 25.3                                       | 16.7                                       |                                      |

See the footnote in Table 1